THESIS

MODELING HIGH PRESSURE FLOW THROUGH AN ORIFICE WITH REAL GAS EFFECTS

Submitted by

Weston Dall

Department of Mechanical Engineering

In partial fulfillment of the requirements

For the Degree of Master of Science

Colorado State University

Fort Collins, Colorado

Summer 2025

Master's Committee:

Advisor: Wade Troxell

Doug Fankell
Kamran Eftekhari Shahroudi

ABSTRACT

MODELING HIGH PRESSURE FLOW THROUGH AN ORIFICE
WITH REAL GAS EFFECTS

Mass flow control of compressible fluids is integral to several industry sectors, including aerospace, defense, research, and energy. Control valves are a common method of mass flow control and regulate a wide variety of fluid flows, including in the food industry, chemical processing, oil and gas refinement, fuel admission to engines and turbines, pharmaceuticals, and other use cases. Currently, leading controls manufacturers commonly regulate large volume fluid flow up to around 1000 psia within 2 percent accuracy by utilizing flow prediction equations and calibration. The Isentropic Compressible Flow Equation is one commonly used method of doing this, and for this thesis is used as a baseline for current prediction methodology.

In high-pressure regimes (i.e., above 1000 psia), compressible fluids begin to deviate significantly from ideal behavior due to a phenomenon known as real gas effects. This thesis seeks to answer how compressible mass flow through an orifice can be accurately characterized at pressures above 1000 psia. To do this, existing methods and their potential for inaccuracy at high pressure are examined. A more accurate method of prediction utilizing a solver and a large fluid property library is proposed and utilized in conjunction with the existing Isentropic Compressible Flow Equation (a commonly used flow equation) to understand the deviation between the two methods. Significant deviation between methods was found to exist especially among gasses with a less ideal molecular structure. Methane displays a deviation of more than

30% in real mass flow when compared to a baseline made by the Isentropic Compressible Flow Equation. Using the solver, a final method of prediction involving use of “ratio maps” combined with the existing Isentropic Compressible Flow Equation was identified as an accurate method of mass flow prediction given knowledge of the gas flow conditions.

This approach shows the capability to solve the problem of predicting mass flow through orifices at pressures greater than 1000 psia. This answers the fundamental question of this thesis and has potential as a high-pressure flow modeling solution for industry and academic applications.

Another significant part of the work done in this thesis involves the identification of holes in the existing knowledge of high-pressure flow prediction and regulation. This involves both a study of existing research and determination of areas in which it is not deep and developing a solution to fix the holes in existing research for mass flow prediction. The development of a potential solution allows for the identification of challenges with this strategy and possible improvements to be made on it. In this thesis, this mainly involves understanding the existing research done on high pressure flow and the relative lack of 1-2 percent accurate flow modelling for high pressure compressible flow in a control valve context. Solution improvements include items such as accounting for potential viscosity effects, improving the prediction of the point at which sonic flow begins, and general improvements to the tools used to make the flow calculations. The need for real test data at high pressures was also very much emphasized in the process of this thesis. Real test data would prove out the method presented here and offer final validation.

TABLE OF CONTENTS

LIST OF FIGURES

LIST OF EQUATIONS

LIST OF ACRONYMS

1. CFE – Isentropic Compressible Flow Equation
2. ISA – International Society of Automation
3. NASA – National Aeronautics and Space Agency
4. NIST – National Institute of Science and Technology
5. REFPROP – REFerence fluid PROPerties
6. EES – Engineering Equation Solver
7. MATLAB – MATrix LABoratory

CHAPTER 1: INTRODUCTION

1.1 Use Cases for High Pressure Flow Prediction

Precision modeling and prediction of mass flow of compressible fluids at extreme pressures is a field of physics that is relatively young when compared to classical thermodynamics largely due to the difficulty of creating physical systems that require and can handle these types of pressures. Most current applications of compressible flow prediction at extreme pressure fall into the categories of industrial, aerospace, defense, and research usage. For the purposes of this thesis, industrial applications centered on precision mass flow metering at high pressures will be focused on.

1.2 Basics of Control Valve Systems

Before examining the applications of precision mass flow prediction and metering, it is helpful to understand the basic function of a control valve. The overarching system a metering valve is used in at a basic level involves a higher-pressure reservoir attached to a lower-pressure reservoir by some penetrable flow obstruction which is often variable. This pressure differential across the flow obstruction causes fluid flow through the flow obstruction. A metering valve is essentially a type of variable flow obstruction. The basic function of a metering valve is to regulate mass flow between this higher-pressure reservoir and the lower pressure reservoir. This is generally accomplished by adjusting the size of a port with some area that separates two parts of a pipe that the working fluid inhabits. A very basic system diagram is displayed below in Figure 1.

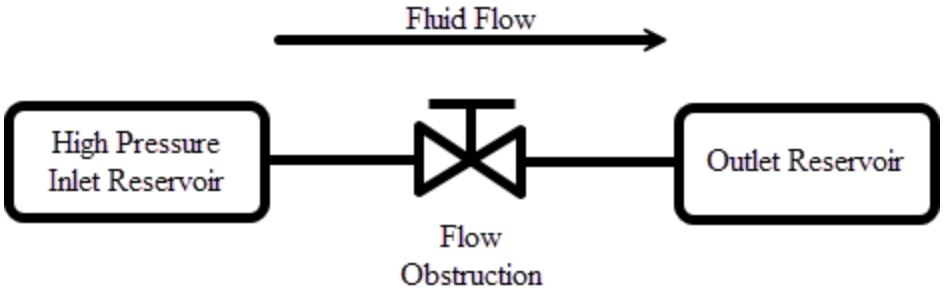

Figure 1 - Simple Metering Valve System

Utilizing this basic idea, effective flow control of the working fluid can be established. Leading industrial control systems manufacturers combine this type of system with precision measurement of flow conditions and precise flow area control. Using these strategies, mass flow can be controlled within 1-2 percent of a desired flow rate. An example of this type of system is shown in Figure 2. In this case, the high-pressure reservoir discussed above consists of the area downstream of the upstream throttling valve. The temperature sensor and pressure tap upstream of the metering valve and the pressure tap downstream of the metering valve provide information that when combined with governing equations and models allow very precise flow prediction. When combined with a metering port whose size can be very precisely controlled, the aforementioned mass flow control within 1-2 percent of a desired value can be realized.

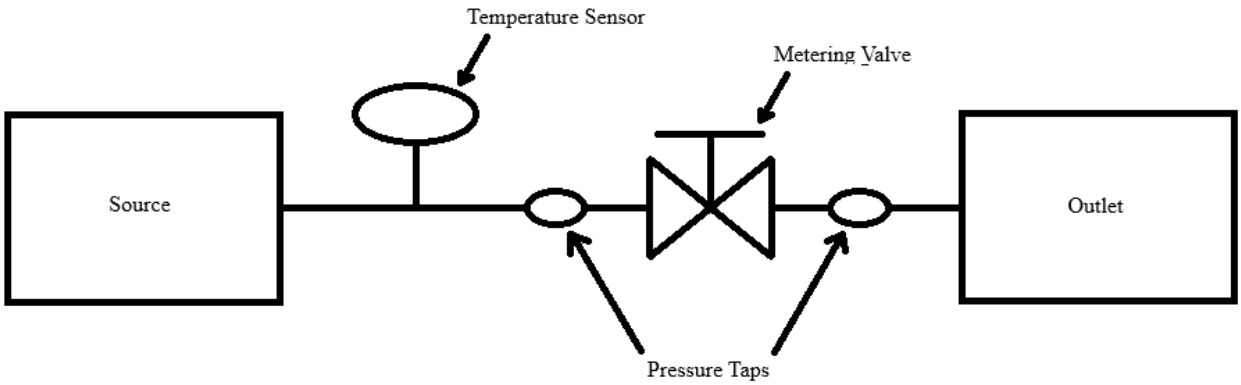

Figure 2- Basic Metering Valve System with Pressure and Temperature Monitoring

1.3 Industrial Application of Control Valve Systems

One prominent use for mass flow control valves is in the region of power generation. Industrial power generation is a massive industry and is an integral part of the modern global economy. This industry is constantly changing and improving, however, there are several mainstream methods for generating power that meet the majority of the world's need for electrical energy. Energy sources for power generation principally include natural gas, coal, nuclear energy, wind and solar energy, and hydropower. The largest of these in the United States are, respectively, natural gas by a significant margin (20%), then nuclear power, then coal, and lastly, renewables and fuel oils [1]. In the United States, natural gas power production exceeded coal production relatively recently (circa 2015) due to the increasingly prevalent desire to move away from coal energy for a variety of environmental and other reasons. This shift has caused an increased focus on making natural gas production more efficient, triggering advances in harvesting natural gas and utilizing it. Most relevant to this thesis are methods of utilizing natural gas as metering valves like the ones described above are frequently used turbine as control

valves for the various points of flow control on the turbine. Natural Gas Turbines are also capable of running at pressures where super compressibility effects take place to a greater degree. This is especially true of supercritical CO_2 cycles.

Supercritical CO_2 cycles have a variety of advantages and challenges when compared with most natural gas turbines employed currently. Their principal benefits are their potential efficiency and ability to provide nearly pure CO_2, which makes complete carbon capture possible, resulting in an emissions footprint that is far more appealing than conventional methods. As governments move towards increased environmental regulation, this second point may become increasingly important for spurring the use of these types of cycles. The largest reason that supercritical cycles are not already mainstream is due to their technical challenges. In addition to all the basic costs of researching and refining new thermodynamic processes like supercritical CO_2 cycles, they can employ extremely high-pressure compressible fluids, which are not traditionally worked with in the natural gas turbine power generation space. This results in several engineering complications. One of these challenges is the need for precision metering valves capable of surviving and precisely controlling compressible fluid flow of various fluids at pressures reaching up to 6000 psia.

At these pressures, modelling gas flow precisely becomes challenging due to significant deviation in the fluid properties from ideal gas behavior. Prediction of mass flow based upon effective flow area and flow conditions (inlet/outlet pressure, temperature, and gas properties at these temperatures and pressures) is critical to effectively controlling this type of system and providing the proper rate of mass flow. The question addressed by this thesis involves this prediction, and specifically how it is affected by extremely high-pressure flow conditions. The isentropic compressible flow equation mentioned above makes some assumptions about how

fluid will act at these pressures that appear to begin to diverge from reality at high pressure. The results of this thesis suggest this divergence may grow significantly at pressures over 1000 psia for most gases and especially for methane, a commonly used fuel and a common application of precision metering valves. Findings suggest error values for the existing method of nearly 24% at 6000 psia and 5 °F.

1.4 Thesis Question

This thesis seeks to address the challenge of accurately (1-2 percent error) characterizing and predicting mass flow of various compressible fluids through a metering valve (in this case defined as some pressure differential across a variable orifice) at high inlet pressures (6000 psia). While current models predict mass flow with high confidence at or below 1000 psia, initial investigations suggest significant deviations (10% flow or more) may result from real gas effects at higher pressures. These real gas effects can be hard to predict with the same accuracy using existing closed-form methods. This research will explore these deviations and develop improved models for high-pressure applications.

To accomplish this goal, a standard method of mass flow calculation used by industry and academia will be compared to an alternative method that has better capability to account for the deviation from ideal behavior that high pressures induce. These methods are compared in "ratio maps" that consist of a ratio of the more "real gas" capable method to the standard method at varying flow conditions. In an end-use application where the user is seeking to predict flow at high pressures, these ratio maps can be used in conjunction with the existing method to create a final flow value that better accounts for high-pressure gas effects.

This thesis is organized into several sections to assist in presenting the content in a logical manner. The first section (which is at its close) is the introduction in which the basics of high-pressure flow and control valves are examined. The introduction gives background and introduces the thesis question which is the basis and guide for the thesis as a whole. The next major section, CHAPTER 2: Background, presents current approaches to compressible mass flow prediction and some of its challenging facets such as real-gas effects and application to real control systems. CHAPTER 3: Approach, details the solution approach taken in this thesis including the mathematical assumptions used and the software and strategy which leveraged these assumptions to create a modelling tool capable of creating an improved mass flow prediction solution. CHAPTER 4: Results examines the product of the solver explained in Chapter 3 and puts context to its various facets including the effect of gas type on real gas correction, the influence of pressure, temperature, and pressure ratio on the differential between the improved and existing method, and some of the potential problems with the solver method. CHAPTER 5: Discussion, explains some of the validation work that was conducted to ensure that the solver operates accurately in regions where real test data has been collected. It also speaks on the significance of the results given in Chapter 4 for industry and high accuracy mass flow prediction. CHAPTER 6: Conclusion and Future Work, ties the other sections into a concise ending and offers clear resolution to the thesis question. This chapter also includes ideas for further improvement and testing of the methodology in this thesis.

CHAPTER 2: BACKGROUND

2.1 The Current Approach to Compressible Flow Prediction

The basic philosophies of modern thermodynamics were largely developed in the early to mid-1800s. The modern field of mechanical engineering is rooted in the utilization of the principles of thermodynamics to accomplish various tasks, often with the use of complex mechanical systems such as HVAC, reciprocating engines, refineries, and turbines. Because of these factors, the fundamental principles of thermodynamics are very well proven and tested by a wide variety of sources. During the time between the discovery and characterization of the basic principles of thermodynamics and today, a large amount of work has been done to manipulate and combine these principles into useful equations and relationships that can be used to characterize various phenomena. Several numerical methods have also been applied to this problem in various forms.

2.2 Existing Methods and Applications

It is helpful to examine existing methods of mass flow prediction at extreme pressures to gather an idea of holes in current knowledge and what already exists. In comparison to flow in lower pressure regions, there are relatively few sources of real flow test data at the pressures of interest here. This is mostly because there are very few labs capable of running tests at such high pressures and a general lack of need for prediction in this regime. Consequently, little exists for controlling flow with extreme precision at these pressures. Due to this, precise flow control based on flow prediction has largely been avoided. Instead, most strategies of regulating flow at extreme pressures have involved a control valve that relies not on prediction but reaction using precision flow measurement and a feedback loop. This lack of flow data and existing control

strategies at pressures near or above 6000 psia is one of the principal reasons for the creation of the model presented in this thesis. Despite this there are other areas of research that hold relevance. Although there is a lack of directly applicable test data, there are a few models for compressible flow through some area at high pressure and some adjacent test data sets that offer insight into possible solutions and provide information on the validity of the solution proposed in this thesis.

2.2.1 Applicable Models

Despite the lack of real test data and models that adequately extend to these pressures, some critical flow models that can be extrapolated to extreme pressures exist. It is not relevant to do a deep study of each method here but briefly examining a few models is helpful. In summary, these flow models make assumptions that make them less relevant or inaccurate for the type of application being discussed here. Generally, they do not appear to be validated via physical results on high pressure applications or finding do not show them capable of the low level of error desired for this thesis.

The first and likely most applicable research on critical flow of compressible fluids through a nozzle was conducted by R.C. Johnson and NASA in the 1960s [2]. Johnson published several academic papers detailing the flow of fluid and specifically natural gas and hydrogen through critical flow nozzles. Johnson develops several proposed equations of state for natural gas in his work which can be used to calculate the properties of the gas such as the critical flow factor C*, compressibility factor Z, and the specific heats. He also examines the Benedict-Webb-Rubin equation of state for Methane and several other methods of generating fluid properties. This work was utilized in this thesis largely to provide background on the existing methods and areas of potential inaccuracy. Johnson targeted the lack of an adequately calculated

compressibility factor Z and the non-constant specific heats from the inlet to the throat of a critical nozzle for his calculations. Using an integration strategy and some other techniques Johnson does appear to have been able to create a relatively accurate improved equation of state generating most of the properties relevant for calculating critical flow through a nozzle. At the time of his work, this was somewhat groundbreaking however given advances put forward by the National Institute of Science and Technology (NIST) in their Reference Properties Library (REFPROP) fluid properties like those calculated by Johnson are found more accurately by using the REFPROP Helmholtz energy model [3]. With his integration technique, Johnson leveraged these fluid properties as well as some empirically generated sonic flow factors to create models that generated somewhat similar results to those in this thesis. Although, this was done, the results produced by Johnson do not have the advantage of REFPROP's highly accurate equations of state with a depth of empirical testing. REFPROP will be discussed more later in this thesis as it is fundamental to the methodology taken.

A second area of research with potentially applicable results is that of hydrogen fuel cells. Real test data has been taken up to 20 MPa for fuel cell applications. Initially, this appears promising for offering validation for this thesis however, this real test data does not appear to be easily accessible to the public and the 20 MPa results do not apply perfectly to the roughly 40 MPa target in this thesis. Despite this, the results of this research do offer some level of confirmation for the findings here. The model used in a paper on "Flow Characteristics of High-Pressure Hydrogen Gas in the Critical Nozzle" appears to essentially account for real gas effects to the extent of using Z, the compressibility factor [4]. It does not appear to account for real gas effects more significantly than that which on a very high level should make it susceptible to the same inaccuracies the compressible flow equation has. Interestingly, the paper states that the

results of its modelling gave a value for flow lower than that of real experimental flow at high pressures (20 MPa or 2900 psia). The source states, “It is interesting to note that the experimented data show a higher coefficient of discharge than unity,” which indicates that the experimental data showed higher flow than would be expected for a sonic nozzle given their models predictions based on experiment conditions. As will be explained later, flow values for the improved method of prediction in this thesis indicate that a sonic flow nozzle will flow roughly 8% more hydrogen gas than existing methods using only the compressibility factor without some of the other real-gas correction factors as the model in this source does. Given these two facts, it offers a loose correlation between the model presented in this thesis and real experimental data. Given an inability to locate this experimental data thus far, this correlation is included nowhere else in this thesis for validation as it is somewhat unconfirmed. Investigating this further is an area of future work.

Another source of real high pressure test data is the atomic energy field. Due to the need to accurately predict the blowdown of ruptured piping in reactors, blowdown data exists ranging up to roughly 37 MPa. Making it less applicable for the purposes of this thesis, it appears to deal largely with multiphase fluids such as depressurizing supercritical water [5]. This makes the research less relevant here as this thesis is dealing exclusively with single phase fluids.

Work has also been done on the evaluation of polytropic efficiency for compressors up to 6000 psi. Although the source this was found in does not appear to contain information for flow through an orifice, “Compressor Performance and Thermodynamics” reaffirms the Helmholtz equations of state as the most accurate and usable source of fluid properties, in this case equations of state based on Helmholtz energy developed by the Groupe Européen de Recherches

Gazières (GERG) instead of NIST [6]. Although the GERG and NIST methods differ in governing agency, initial investigation indicates they do not differ in substance significantly.

The Colorado Engineering Experiment Station has done relatively similar research however its research reaches up to roughly one third of the 6000 psia target here making it less relevant [7]. In a publication they published on the Isentropic coefficient (which is named as k, the ratio of specific heats for this thesis) and the viscosity of various fuel gasses, pressures of around 12 MPa or 1740 psia were reached. The Colorado Engineering Experiment Station, shows the validity of REFPROP, comparing it to real test data to ensure its validity.

2.3 Isentropic Flow Equation Derivation

Although these methods do offer some minor assistance in the area of high-pressure flow prediction they cannot fulfill the need for flow prediction perfectly, especially not in the context of the 1-2% accuracy at 6000 psi sought by industry. Before moving to the methods developed in this thesis, an understanding of the existing flow prediction methods in industry is key. Currently, for many of the leading industrial users of compressible flow prediction, a flow equation based on some known fluid properties and thermodynamic assumptions that can be found in a college thermodynamics book is used [8]. Due to its use of the isentropic assumption and compressibility factor Z, this equation will be dubbed the Isentropic Compressible Flow Equation for the remainder of this thesis. Additionally, this will sometimes be abbreviated as the CFE (Compressible Flow Equation). On a high level, this equation is based around a system involving a fluid flowing through some upstream pressure vessel (e.g. an inlet pipe), an orifice with some effective area, and a downstream pressure vessel (such as an outlet pipe). It sets up a relationship between mass flow rate and effective flow area, generally with input knowns upstream pressure P1, downstream pressure P2, upstream temperature T, specific gravity of the

fluid relative to air SG, compressibility of the fluid Z, and the ratio of specific heats of the fluid k. To understand the function of this equation and to gain an understanding of where its largest inaccuracies lay, a derivation is useful. The derivation of the isentropic compressible flow equation can be found below.

The first major principle of the isentropic compressible flow equation is the conservation of energy. Essentially, all the internal and kinetic energy of the fluid at the inlet is equal to the kinetic and internal energy of the fluid at the outlet. This takes the form of enthalpy and velocity.

$$h_{inlet} + \frac{V_{inlet}{}^2}{2} = h_{outlet} + \frac{V_{outlet}{}^2}{2} \qquad (1)$$

If the orifice metering the fluid in the pipe is allowing fluid to pass through it from the inlet, the fluid upstream is, by definition, flowing, given no other escape path exists. Despite this fact, the upstream velocity of the fluid is far smaller than the fluid velocity downstream of the orifice and given normal flow conditions for almost any metering or small orifice. This discrepancy between velocities is generally so small that it can be ignored and assumed to be zero. This is one potential inaccuracy of this equation however it is generally a small one given the orifice in the fluid path is significantly smaller than the inlet fluid path or pipe. Thus, the following equation can be formed given the energy balance equation, setting v_{inlet} to zero and moving outlet enthalpy to the left side of the equation.

$$h_{inlet} - h_{throat} = \frac{V_{throat}{}^2}{2} \qquad (2)$$

The next major assumption to be introduced and utilized for this equation is the assumption of constant specific heats. This is another source of inaccuracy of this model and is likely the cause of significant deviation from real gas behavior at extreme pressure and

temperature differentials between the inlet and outlet of the orifice. Using this assumption, $h_{inlet} - h_{throat}$ can be exchanged for $C_p(T_{inlet} - T_{throat})$ forming the equation below.

$$C_p(T_{inlet} - T_{throat}) = \frac{{V_{throat}}^2}{2} \qquad (3)$$

This can then be combined via the term for velocity at the orifice throat with the mass flow equation for flow through some cross-sectional area.

$$\dot{m} = \rho_{throat} V_{throat} A_{throat} \qquad (4)$$

When the square root is taken the simplify the equation this becomes the following.

$$\dot{m} = \rho_{throat} A_{throat} \sqrt{2C_p(T_{inlet} - T_{throat})} \qquad (5)$$

Once T_{inlet} is factored out this equation takes the following form in which the isentropic relationship between inlet/outlet pressure and inlet/outlet temperature can be taken advantage of to make the equation non-requiring of the input of T_{throat}.

$$\dot{m} = \rho_{throat} A_{throat} \sqrt{2C_p T_{inlet} \left(1 - \frac{T_{throat}}{T_{inlet}}\right)} \qquad (6)$$

The following isentropic relationships are introduced.

$$\left(\frac{T_{throat}}{T_{inlet}}\right) = \left(\frac{P_{throat}}{P_{inlet}}\right)^{\frac{k-1}{k}} \qquad (7)$$

$$\left(\frac{\rho_{throat}}{\rho_{inlet}}\right) = \left(\frac{P_{throat}}{P_{inlet}}\right)^{\frac{1}{k}} \qquad (8)$$

Substituted into the equation for mass flow developed above, they form the following equation.

$$\dot{m} = \rho_{inlet}\left(\frac{P_{throat}}{P_{inlet}}\right)^{\frac{1}{k}} A_{throat}\sqrt{2C_pT_{inlet}\left(1-\left(\frac{P_{throat}}{P_{inlet}}\right)^{\frac{k-1}{k}}\right)} \qquad (9)$$

This can be simplified to the form below

$$\dot{m} = \rho_{inlet}A_{throat}\sqrt{2C_pT_{inlet}\left(\left(\frac{P_{throat}}{P_{inlet}}\right)^{\frac{2}{k}}-\left(\frac{P_{throat}}{P_{inlet}}\right)^{\frac{k+1}{k}}\right)} \qquad (10)$$

This then simplifies to a form that leverages ideal gas properties to eliminate the need to solve for C_p and inlet density. These ideal gas properties are below. R is the ideal gas constant.

$$\rho_1 = \frac{P_{inlet}}{RT_{inlet}} \qquad (11)$$

$$C_p = \frac{kR}{k-1} \qquad (12)$$

Substituting these into the latest mass flow equation, we can establish the following equation.

$$\dot{m} = \frac{P_{inlet}A_{throat}}{RT_{inlet}}\sqrt{\frac{2kRT_{inlet}}{k-1}\left(\left(\frac{P_{throat}}{P_{inlet}}\right)^{\frac{2}{k}}-\left(\frac{P_{throat}}{P_{inlet}}\right)^{\frac{k+1}{k}}\right)} \qquad (13)$$

This simplifies further by moving R and T_{inlet} under the radical.

$$\dot{m} = P_{inlet}A_{throat}\sqrt{\frac{2k}{(k-1)RT_{inlet}}\left(\left(\frac{P_{throat}}{P_{inlet}}\right)^{\frac{2}{k}}-\left(\frac{P_{throat}}{P_{inlet}}\right)^{\frac{k+1}{k}}\right)} \qquad (14)$$

SG, or specific gravity, is frequently used in conjunction with the gas constant for air R_{air} in the context of industry to allow for calculations using gasses whose density is most easily defined relative to air. The governing equation from the ideal gas law can be related to this law integrated with SG for air.

$$\frac{P}{RT} = SG\left(\frac{P}{R_{air}T}\right) \qquad (15)$$

This can then be reworked so that R can be found in terms of R_{air} and SG.

$$R = \frac{R_{air}}{SG} \qquad (16)$$

Substituting this back into the mass flow equation, the following can be obtained.

$$\dot{m} = P_{inlet}A_{throat}\sqrt{\frac{2kSG}{(k-1)R_{air}T_{inlet}}\left(\left(\frac{P_{throat}}{P_{inlet}}\right)^{\frac{2}{k}} - \left(\frac{P_{throat}}{P_{inlet}}\right)^{\frac{k+1}{k}}\right)} \qquad (17)$$

Finally, a constant K_1 is introduced to fix dimensional consistency and to account for the constants in the equation. For units of mass flow in lbm/hr, the value of K_1 is shown below.

$$K_1 = 3594\frac{(lbm)}{(hr)*\sqrt{\frac{1}{^\circ R}}(lbf)} \qquad (18)$$

Adding this to the mass flow equation from above, we get the following equation for an ideal isentropic gas.

$$\dot{m} = K_1P_{inlet}A_{throat}\sqrt{\frac{kSG}{(k-1)T_{inlet}}\left(\left(\frac{P_{throat}}{P_{inlet}}\right)^{\frac{2}{k}} - \left(\frac{P_{throat}}{P_{inlet}}\right)^{\frac{k+1}{k}}\right)} \qquad (19)$$

This equation can be improved with the use of compressibility factor Z. Z essentially describes the deviation of a real gas from ideal behavior, specifically in its compressibility. The equation

defining it is given below. P denotes pressure, V denotes volume, and n, R, and T denote the number of moles, the ideal gas constant, and temperature, respectively.

$$Z = \frac{Pv}{nRT} \qquad (20)$$

or

$$Pv = ZnRT \qquad (21)$$

Z is a fluid property and can be incorporated into the definition of enthalpy by substituting

$$h = u + Pv \qquad (22)$$

$$h = u + ZnRT \qquad (23)$$

$$dh = du + ZRdT \qquad (24)$$

C_p and C_v can then be introduced for dh and du.

$$C_p dT = C_v dT + ZRdT \qquad (25)$$

And dT removed.

$$C_p = C_v + ZR \qquad (26)$$

Substituting in $k = \frac{C_p}{C_v}$.

$$C_p = \frac{ZR}{k-1} \qquad (27)$$

This can then be substituted into the ideal isentropic equation to account for compressibility. C_d or Coefficient of Discharge multiplied by geometric area $A_{geometric}$ can also be substituted in for A_{throat} to allow the use of the more easily measured geometric area and C_d. Given these, the final equation is:

$$\dot{m} = K_1 P_{inlet} A_{geometric} C_d \sqrt{\frac{kSG}{(k-1)T_{inlet}Z}\left(\left(\frac{P_{throat}}{P_{inlet}}\right)^{\frac{2}{k}} - \left(\frac{P_{throat}}{P_{inlet}}\right)^{\frac{k+1}{k}}\right)} \qquad (28)$$

By definition, a sonic flow condition occurs when properties of the downstream fluid in a fluid flow no longer affect the upstream fluid flow. To allow the above equation to operate in the sonic region, constant $R1$ can be substituted for $\frac{P_{throat}}{P_{inlet}}$. The derivative of mass flow $\dot{m}$ with respect to this constant $R1$ can be taken and set to zero to find the point at which mass flow becomes unaffected by downstream pressure conditions. Once $R1$ is substituted in and $(\frac{\partial \dot{m}}{\partial R1})$ is set to 0, we can simplify to the following.

$$0 = \frac{2}{k}(R1)^{\frac{2}{k}-1} - \frac{k+1}{k}(R1)^{\frac{k+1}{k}-1} \qquad (29)$$

Doing this, $R1$ comes to the following in terms of k.

$$R1 = \left(\frac{2}{k+1}\right)^{\frac{k}{k-1}} \qquad (30)$$

This results in the final form of the isentropic equation where $R1$ is set to $\frac{P_{throat}}{P_{inlet}}$ for subsonic cases and set to $\left(\frac{2}{k+1}\right)^{\frac{k}{k-1}}$ for sonic flow conditions. Based on the definition of $R1$ the following is the full Isentropic Compressible Flow Equation used for a large portion of precision mass flow prediction.

$$\dot{m} = K_1 P_{inlet} A_{geometric} C_d \sqrt{\frac{kSG}{(k-1)T_{inlet}Z}\left((R1)^{\frac{2}{k}} - (R1)^{\frac{k+1}{k}}\right)}$$

where:

$R1 = \left(\frac{2}{k+1}\right)^{\frac{k}{k-1}}$ when $\frac{P_{throat}}{P_{inlet}} < R1$ (sonic flow conditions exist)

and

$R1 = \frac{P_{throat}}{P_{inlet}}$ when $\frac{P_{throat}}{P_{inlet}} \geq R1$ (subsonic flow conditions exist)

(31)

2.4 Benefits of the Isentropic Compressible Flow Equation

This form of the isentropic equation has several benefits. It requires relatively few input variables, all of which are generally accessible given relatively common tools of fluid measurement such as pressure transducers and thermocouples. International Society of Automation (ISA) and American National Standard Institute (ANSI) are standards for measuring the flow of gas through control valves or other orifices and their measurement. International Standards Association document 75.02.01 “Control Valve Capacity Test Procedures” details a setup for testing the flow of compressible fluids through an orifice or “test specimen” to determine its flow characteristics (generally, this is the effective area or some other combination

or measure of geometric flow area and coefficient of discharge). This setup is shown in the figure below.

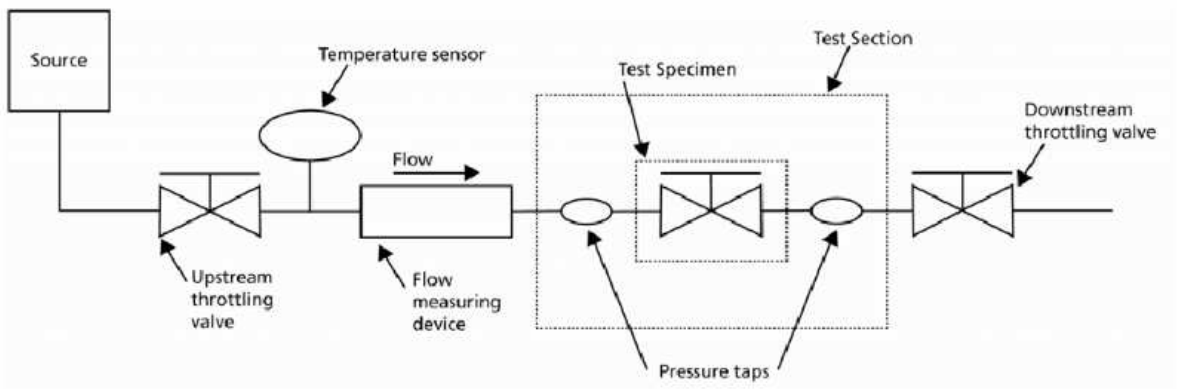

Figure 3 - Flow Testing Setup

The sensors required for accurate flow testing have developed somewhat in response to the needs of equation(31)or of those like it; however, in the above diagram, the sensors installed in the system collect exactly the information needed to solve for effective flow area in the equation above. The remaining variables in Equation 1 needed to predict the flow area are generally attainable given a knowledge of the fluid and some constant k, SG, and Z for it or, more accurately, a lookup table for the fluid that can provide these constants given the pressure and temperature of the fluid. Additionally, this equation has been proven accurate to less than 2 percent deviation by leading industrial manufacturers of control valves using precision flow meters. It is also closed form and can be easily incorporated into a variety of software that can run basic math calculations. For example, a Visual Basic implementation of the isentropic equation is shown below in Figure *4*. This equation is incorporated into an Excel macro.

```
'FUNCTION AEFF
'This function yields ACd given flow, pressure, and gas conditions

Public Function Aeff(Wf#, p1#, p2#, k#, t#, sg#, z#) As Double

Dim R7 As Double

'Determination of R7 term (choked/ unchoked)
    If p2 / p1 >= (2 / (1 + k)) ^ (k / (k - 1)) Then
        R7 = p2 / p1
    Else
        R7 = (2 / (1 + k)) ^ (k / (k - 1))
    End If

'Flow formula
   Aeff = Wf / (3955.289 * p1 * Sqr(((k * sg) / ((k - 1) * (t + 459.67) * z)) * ((R7 ^ (2 / k)) - (R7 ^ ((1 + k) / k)))))

End Function
```

Figure 4 Visual Basic Implementation of the Isentropic Compressible Flow Equation

Because of its relatively easy use and high accuracy, the isentropic compressible flow equation displayed in Equation 1 has become a standard for industry and research institutions.

2.5 Supercompressibility Effects

A large amount of literature exists around systems utilizing the above set of equations and other similar systems. Generally, flow through orifices, and especially nozzles (here considered a variety of orifice), has been well explored due to a variety of reasons at pressures extending to around 1000 psia. As stated previously, applications can range from gas flow control in industrial processes to fluid flow modeling on spacecraft. In large part, this literature deals with compressible fluid flow at pressures below where real gas effects have a significant effect. This lack of literature and relative lack of study is largely due to the specialized equipment needed to test at these pressures and the relatively small need to precisely understand what gas does at these pressures in the context of flow through an orifice or nozzle.

Despite the higher prevalence of literature and studies describing gas flow at pressures below 1000 psia, some work has been done to describe gas in the region above 1000 psia. When combined with the core principles of thermodynamics, this can be very useful in characterizing

compressible flow and determining the effect super compressibility can have on gas flow metering.

The external resources used for this thesis come from documentation and work produced by a variety of sources; however, the most important contributors include the National Institute of Science and Technology, the National Aeronautics and Space Administration, and the American Society of Mechanical Engineers. The first of these, the National Institute of Science and Technology (NIST), dealt mainly with the characterization of gas properties at extreme pressures. NIST has done a great deal of work in this area, and their tool/library named REFPROP (reference properties) is generally considered the industry standard for data of this type. REFPROP is based on an extensive set of empirical testing done by several sources that has then been conglomerated into a single data source. REFPROP libraries contain a variety of fluid properties. To name a few, these include density, compressibility factor, quality, phase, C_p, heat of vaporization, entropy, enthalpy, and chemical potential. Each of these data types is built out for a wide variety of fluids ranging from fuels to refrigerants across a relatively vast pressure and temperature range. NIST has also built a wide variety of ways to access REFPROP, including an Excel tool and tie-ins to Engineering Equation Solver. Both are used extensively in this thesis. These uses will be explained in later sections.

2.6 Real Gas Effects

In the above derivation, the compressible flow equation utilizes several ideal gas relationships and makes some assumptions that cause it to be susceptible to real physics that occur in real gas specimens. The ideal gas laws and assumptions are fundamentally designed around a single atom gas that does not display some of the complex intermolecular forces that real gasses (and especially real gasses consisting of larger molecules display). When these ideal

gas models are used on gasses at relatively low pressures, they can achieve the relatively high accuracy described above. Of interest to this thesis, this conformance to ideal gas behavior rapidly begins to break down when gas pressure increases due to the increased proximity of the gas molecules to each other. This non-conformance to ideal behavior is generally termed “real gas effects”.

2.6.1 Helmholtz Energy

Several different methods have been put together to help compensate for these effects. As mentioned previously, one method, which is now somewhat less used for this, was developed by R.C. Johnson. Johnson was examining the effects of real gas properties on high pressure flow through nozzles in conjunction with the National Aeronautics and Space Agency (NASA). Johnson’s approach to the problem essentially involved the use of ideal gas properties combined with an overlay of empirically generated equations of state that categorized the effects of real gas. This approach was relatively effective but utilized a strategy involving integration that cause it to be less favored in comparison to newer approaches of real gas effect description.

Johnson predicted gas properties in pressure and temperature regions that cause real gas effects to take a larger role; however, as mentioned, his methods have complications largely in actual computation. Despite this, the idea of mapping out fluid properties for a large range of pressure and temperature conditions was a key step for accurate compressible mass flow prediction. Currently, the most widely used precision method for determining fluid properties in regions where real gas effects have a significant influence involves a method using “Helmholtz Energy”. The use of Helmholtz Energy for the prediction of fluid properties essentially involves the calculation of the ideal portion and the real gas portion of a fluid’s total energy. Using this calculated energy, partial derivatives can then be used to generate relevant fluid properties such

as the ratio of specific heats k, compressibility Z, Mach number c, and a variety of other relevant fluid properties.

This strategy produces accurate and useful results in the region of fluid property prediction, especially when going to extreme pressures. The REFPROP tool made by NIST for fluid properties described above is fundamentally based on the Helmholtz Energy strategy. REFPROP was essentially created to make access to the Helmholtz more convenient and reliable. REFPROP's libraries extend far into high-pressure regions (2000MPa or almost 300,000 psia) with relatively high accuracy. This is variable across the data set, but most comparisons of the fluid properties generated to real test data are within one percent accuracy.

CHAPTER 3: APPROACH

3.1 Assumptions

The central aim of this thesis is to answer the question of how flow through an orifice can be characterized in systems where supercompressibility effects due to extreme gas pressures have potential to cause significant deviation from more ideal behavior. To accomplish this goal, an improved method of prediction better at accounting for real gas effects had to be created. This method then was compared back to existing methods both for validation at low pressures and for information gathering of what deviation might be expected at high pressures. To create this improved method, the underlying assumptions of the Isentropic Compressible Flow Equation were examined, and improvements were made where possible.

Assumptions are, in many ways, the root of the problems with past methods of predicting compressible flow through orifices. As with most mathematical models, improvement can be produced by eliminating assumptions that are not entirely accurate. This was the fundamental idea of the approach for producing a more accurate method of predicting flow through an orifice in this thesis. Despite this desire/need to eliminate assumptions, the world of modelling physical systems is, at its core, dependent on assumptions. It is not possible to model anything physical mathematically without making and utilizing some assumptions. Because of these two competing factors, the assumptions used to model this thesis were selected carefully. Many of the assumptions used are solid to the point of being more universal principles rather than assumptions; however here they will be called assumptions.

It is a useful to note which core assumptions were used for a more accurate prediction strategy. The first assumption is the conversion of a fluid's internal energy into kinetic energy.

This is a known thermodynamic principle relying on the fundamentals of the conservation of energy. This basic equation is used for both the inlet to the stagnation states and the stagnation to throat states. A major assumption here is that all the fluid energy begins as enthalpy and no velocity. Essentially, the fluid is assumed to stop completely before it enters the orifice throat. In general, this assumption is true enough to cause negligible error. Generally, the fluid speed after the nozzle nears or is the fluid speed of sound. This is usually much greater than the fluid inlet speed. For the purposes of the results shown below, this assumption was essentially made artificially true and essentially filtered out by modeling an inlet pipe diameter that is extremely large, which renders inlet flow velocity negligible.

$$h_{inlet} = h_{outlet} + \frac{{v_{outlet}}^2}{2} \qquad (32)$$

The second major assumption is the isentropic assumption, which states that the fluid will have the same entropy before and after the orifice. This is also well proven thermodynamically for this type of system and was used because it provides a necessary constraint for the system.

$$s_{inlet} = s_{outlet} \qquad (33)$$

The third major assumption and relationship used in the advanced prediction strategy relies fundamentally on the conservation of mass. One part of this relationship relies on the definitions of area, velocity, and density to make up the outlet mass flow.

$$\dot{m} = \rho * A_{cross-sectional} * v_{oulet} \qquad (34)$$

Another assumption that has significant effects later in the mapping phase is attached to where a subsonic solver method is used instead of a sonic solver method. In the Isentropic Compressible Flow Equation above (Equation 1) the point at which the sonic vs. subsonic solver is utilized is

defined as the point when pressure ratio P_r equals $\left(\frac{2}{k+1}\right)^{\frac{k}{k-1}}$ for the given fluid. This is looked at in detail later in the results section of this thesis however in brief, during the construction of the solver this assumption was used. Examining data output from the solver, there is some evidence that this assumption is faulty in areas where real gas effects have a significant effect.

3.2 Resulting Method

3.2.1 Equations

Assumptions and the mathematical relationships that can be made using them form a basis for creating a physical model of compressible flow moving through an orifice; however, some sort of tool is then needed to combine these relationships into a way to calculate fluid flow based on flow conditions. In past methods discussed here, this was done using basic algebra and the manipulation of equations in combination with fluid properties that are assumed constant through the orifice. To avoid having to use constant fluid properties based solely on the inlet conditions through the orifice, a non-algebraic solver can be used in conjunction with fluid property libraries.

For the purposes of this thesis, the multivariate solver Engineering Equation Solver and its built-in access to the National Institute of Science and Technology's REFPROP library of fluid properties was used to solve a system of equations. Essentially Equation 32 through Equation 34 and several other supporting equations were all set up in the solver to be solved simultaneously.

Figure 5 below contains most of this information. It consists of a clip of the EES solver tool's formatted equations window and holds the complete list of equations used to solve for mass flow. Figure 5 displays the sonic solver equations. The subsonic solver equations

incorporate Mach number into all the places where the speed of sound is used as velocity in the sonic solver. Each of the variables that use EES built-in REFPROP access in figure 4 are formatted with the variable name followed by the input properties needed to determine the fluid property in question. For example, entropy at the orifice throat is specified as

$$s(Gas_{type\$}, T = T_{throat}, P = P_{throat}) \qquad (35)$$

In this case, entropy is being found for the gas "$Gas_{type\$}$" at temperature "$T_{throat}$" and at pressure "$P_{throat}$". All these variables are fed to the solver or determined within it as part of the equation system.

Relationship between static pressure and stagnation temperature for a given recovery factor:

$$T1 = \frac{Tm1 - Rf \cdot To}{1 - Rf}$$

Isentropic relation between stagnation and throat states:

$$\mathbf{s}\left(Gas_{Type\$}, T = T_{throat}, P = P_{throat}\right) = \mathbf{s}\left(Gas_{Type\$}, T = To, P = Po\right)$$

Energy balance between inlet stagnation and critical flow states:

$$\mathbf{h}\left(Gas_{Type\$}, T = T_{throat}, P = P_{throat}\right) + \frac{\mathbf{SoundSpeed}\left(Gas_{Type\$}, T = T_{throat}, P = P_{throat}\right)^2}{2} = \mathbf{h}\left(Gas_{Type\$}, T = To, P = Po\right)$$

Isentropic relation between stagnation and throat states:

$$\mathbf{s}\left(Gas_{Type\$}, T = To, P = Po\right) = \mathbf{s}\left(Gas_{Type\$}, T = T1, P = P1\right)$$

Energy balance between stagnation and inlet states:

$$\mathbf{h}\left(Gas_{Type\$}, T = T1, P = P1\right) + \frac{u1^2}{2} = \mathbf{h}\left(Gas_{Type\$}, T = To, P = Po\right)$$

Conservation of mass between inlet and the critical flow area:

$$u1 = \rho\left(Gas_{Type\$}, T = T_{throat}, P = P_{throat}\right) \cdot \frac{Flow_{Area}}{Inlet_{Area}} \cdot \frac{\mathbf{SoundSpeed}\left(Gas_{Type\$}, T = T_{throat}, P = P_{throat}\right)}{\rho\left(Gas_{Type\$}, T = T1, P = P1\right)}$$

Mass Flow through the throat:

$$\dot{m} = \rho\left(Gas_{Type\$}, T = T_{throat}, P = P_{throat}\right) \cdot \mathbf{SoundSpeed}\left(Gas_{Type\$}, T = T_{throat}, P = P_{throat}\right) \cdot \frac{3600\ [s/hr]}{1000\ [mm/m]^2} \cdot Flow_{Area}$$

Stagnation Compressibility Factor For Output:

$$Zo = \mathbf{Z}\left(Gas_{Type\$}, T = To, P = Po\right)$$

Speed of Sound to Print

$$SpdSnd = \mathbf{SoundSpeed}\left(Gas_{Type\$}, T = T_{throat}, P = P_{throat}\right)$$

Calculate Critical Flow Factor:

$$C^* = \rho\left(Gas_{Type\$}, T = T_{throat}, P = P_{throat}\right) \cdot \mathbf{SoundSpeed}\left(Gas_{Type\$}, T = T_{throat}, P = P_{throat}\right) \cdot \frac{(R \cdot To)^{0.5}}{Po \cdot 1000000\ [Pa/MPa]}$$

$MW = \mathbf{MolarMass}\left(Gas_{Type\$}\right)$ Molecular Mass for Gas Selected

$Ru = 8314.4598$ [J/K-kmol] Universal Gas Constant

$$R = \frac{Ru}{MW}$$ Specific Gas Constant

Figure 5 - Solver Governing Equations

Following this pattern, everywhere fluid properties are required per the equation set, the solver's built-in REFPROP library access is used to find the precise fluid property for the specified application. This means that at the throat of the flow path (the smallest cross-sectional area the

flow passes through), the fluid density is calculated to an exact value using REFPROP instead of by using the isentropic relationship used in past methods

Because of this and the other areas where precise fluid properties are pulled from REFPROP, real gas effects are accounted for, making the solver model more accurate in higher pressure regimes where real gas effects have a greater impact.

3.2.2 Iteration

The goal of this thesis is to predict compressible flow accurately at very high pressures. Given this goal, it is desirable to predict flow at any given set of flow conditions at these high pressures. This presents a challenge as there are a large number of variables that need to be used for this prediction, and prediction is desired at a large number of flow conditions. The above system of equations integrated into EES can create a theoretically more ideal mass flow solution based on input variables; however, if the above equations are all that is used, EES can only be run manually for a single point. To establish trends on a high level, this is impractical as thousands of points would need to be run manually to create data sets which trends can be seen on. Additionally, it is helpful to see these trends based on a comparison to some baseline like the Isentropic Compressible Flow Equation, which would entail manually running both the EES solver and the Isentropic Compressible Flow Equation for every data point.

To overcome these issues, a process flow for data collection was built using a variety of software and subcomponents within them. This process flow was built to be run on large data sets that are relatively easy to generate. The overview of the steps is as follows:

1. Generate input tables containing some number of trial rows, each of which contains a set of flow test cases based upon some gas type, pressure ratio P_r, P_{inlet} and ACd (ACd = 1

for most of the result section below) and k, SG, and Z for the inlet conditions of the gas. Z, SG, and k are generated using a REFPROP Excel add-in.

2. Import this input table into a MATLAB script via a MATLAB built in function referencing the valid excel file path and the specified sheet and cells. Rework this table into another table inside of MATLAB which contains units usable for the EES solver and the Isentropic Compressible Flow written into the MATLAB script.
3. Create a new output file for the results of the solver to be recorded into.
4. Write the input conditions of the first row of the table created earlier into a .dat file that can be imported from by EES.
5. Use a MATLAB built-in tool to run one of two possible command line codes. One if the value of the P_r is less than α which is equal to $\left(\frac{2}{k+1}\right)^{\frac{k}{k-1}}$ using the value of k for that trial, and one if it is greater than or equal to α. This corresponds to which flow cases are sonic and subsonic so the correct solver can be run. Each command line operation runs the EES sonic solver or the EES subsonic solver based on the value of alpha.
6. After the EES solver has been run, it exports its outputs to another .dat file, which is read by MATLAB using a MATLAB built-in function. These outputs are stored in matrices to be added to the final output file. Steps 4 through 6 repeat until mass flow outputs have been generated and stored for every input row.
7. The input conditions initially imported, including k, SG, and Z, are fed through a MATLAB implementation of the compressible flow equation to create a secondary mass flow rate using the Isentropic Compressible Flow Equation. The computation is conducted for all input rows and stored for the output file.
8. A final output matrix is built and written into the Excel output file created in step 3.

Once this set of steps has been completed, the user has a final output file containing a large set of flow conditions and the mass flow, which should each have a corresponding ratio of the EES solver to the Isentropic Compressible Flow Equation. The MATLAB code also creates a percent deviation between the Solver and CFE and a ratio of Solver mass flow over CFE mass flow. To create the visualizations shown below in the results section dubbed “ratio maps”, this ratio of solver to CFE was plotted against the inlet temperature, inlet pressure, and pressure ratio for each trial, creating a surface for each temperature.

CHAPTER 4: RESULTS

4.1 Method Selection

A desired result of this thesis was understanding how high-pressure flow through an orifice can be successfully predicted and characterized. An integral part of the results that a study of this question should produce is an analysis of possible methods, including a characterization of their benefits, costs, and overall functionality. The solver and approach eventually landed on is detailed previously in the "Approach" section of this report; however, it is worthwhile to explain some of the pros and cons of various methods discovered during research into this topic.

Several possible methods were originally explored when trying to determine the best way of predicting flow. The methods were evaluated for a variety of factors, the largest of which were accuracy at high pressures, functionality for use by industry and academia, ease of validation, and ease of implementation and creation. The methods evaluated for accomplishing the task primarily consisted of computational fluid dynamics models, manipulation/improvement of the isentropic compressible flow equation, and a solver based on thermodynamic equations. As is inherent, each of these methods had many different possible implementation options. These were most explored for the solver as this was the method eventually chosen for use for the purposes of this thesis.

A Computational Fluid Dynamics (CFD) solution to this issue would principally entail a software capable of running the calculations required loaded with some 3D model of an orifice. This would then need to be run either by end users for each test case they have or run on some test set up front that generates data which can be interpolated for ACd and flow conditions. This has several inherent and severe challenges. Regarding the concern of accuracy, computational

fluid dynamics simulations have low transparency into their results compared to other methods and are susceptible to a variety of errors in the CAD model, the software, the mesh, and the simulation setup. They are also time-consuming to set up and must be run on a case-by-case basis. For these reasons, this method was not chosen.

Another possible avenue for creating a better prediction method involves the improvement of the isentropic compressible flow equation using some sort of factor or reworking of its equations. Ultimately, this approach is impractical due to the need for significant work involved in creating equations of state or corrections for each gas capable of adapting the isentropic equation to high-pressure applications.

Given the infeasibility of these two methods, the most reasonable method of flow prediction that offers improved accuracy is some sort of solver relying on a combination of fluid property lookup at various locations in the flow process and solid thermodynamic assumptions. As detailed later, this method can also be paired with the existing isentropic flow equation through "ratio tables" that correct it using gas type, inlet pressure, inlet temperature, and pressure ratio.

4.2 Ratio Tables

The aim of this thesis is to answer the question of how flow of a compressible fluid through an orifice of known cross-sectional area and known Cd (coefficient of discharge) can be accurately predicted. To do this in a real physical environment, information about the fluid at the inlet and outlet, information about the physical geometry of the orifice that flow is allowed through, and a method for using this information to predict fluid flow are all needed. This method is discussed in some detail in the approach section of this report. Essentially, this method

consists of using a known and trusted method of prediction (The Isentropic Compressible Flow Equation) that has been proven functional at lower pressures where real gas effects are less impactful and then determining the error between this method and a more accurate solver method. The tool described in the approach section above can accomplish this by essentially exercising the existing and more accurate solver method on a very large set of experimental cases. The method of comparison primarily used for visualizing or understanding the difference between the existing and more accurate solver method in the approach above is a ratio of the solver method divided by the existing method. This will also be referred to as deviation, predicted error, or just error in further explanation.

$$Ratio = \frac{SolverMassFlow}{CompressibleFlowEquationMassFlow} \quad (36)$$

Therefore, the above method primarily consists of a very large set of virtual experiments (made up of a set of flow conditions) and a ratio of comparison between the existing compressible flow equation and the solver method for each case. Several different visualization techniques can be used to see trends in these results, and there are several facets of the trends that are of interest. These facets of interest include the effects of gas type, temperature, pressure ratio (Outlet Pressure/Inlet Pressure), and inlet pressure on the shape and magnitude of the difference between the compressible flow equation and the solver method.

4.2.1 Ratio vs Gas Type

As explained earlier, the relationship between gas type and the ratio of the compressible flow equation to the solver error is useful to understand. Gas type appears to significantly influence the magnitude of the ratio of solver to CFE (Compressible Flow Equation) at various positions. In visualization techniques, this results in a different ratio surface "shape" with a

different overall magnitude. The following graphics depicting the ratio across a range of inlet pressure and pressure ratio for some given temperature demonstrate this. All three “Ratio Maps” seen below were produced using the same set of flow conditions, meaning a large number of virtual experiments using the same inlet pressures, same outlet pressures, same temperatures, and same effective area were run through the Isentropic Compressible Flow Equation and the solver method also described above resulting in the ratios seen below plotted in 3D space via their inlet conditions and resulting ratio.

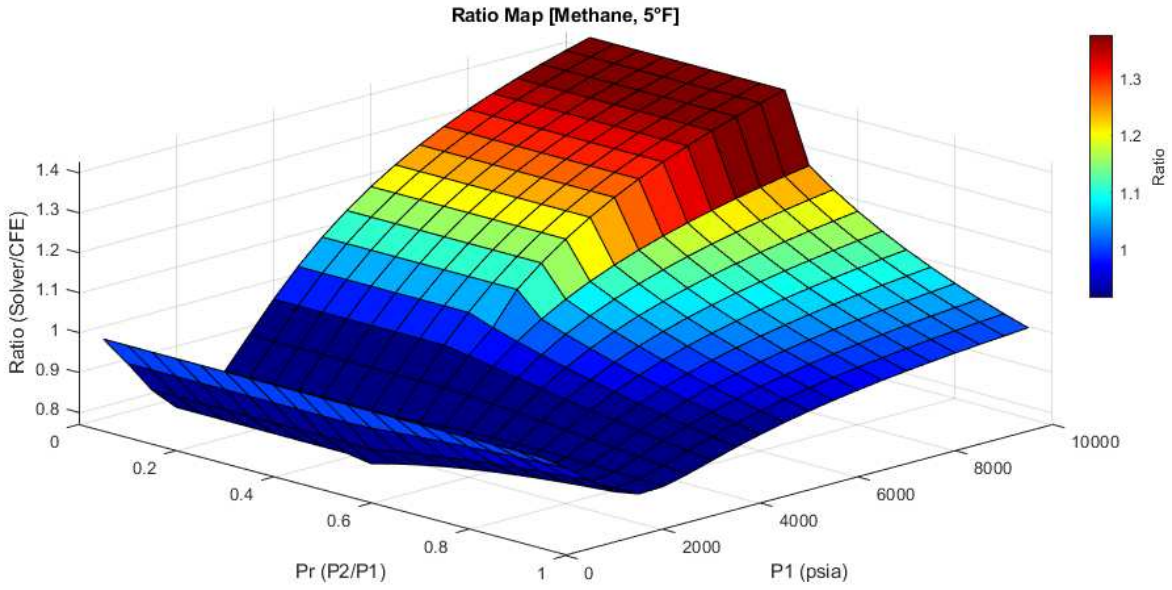

Figure 6 - Methane Mass Flow Ratio v. Pr v. P1 5°F

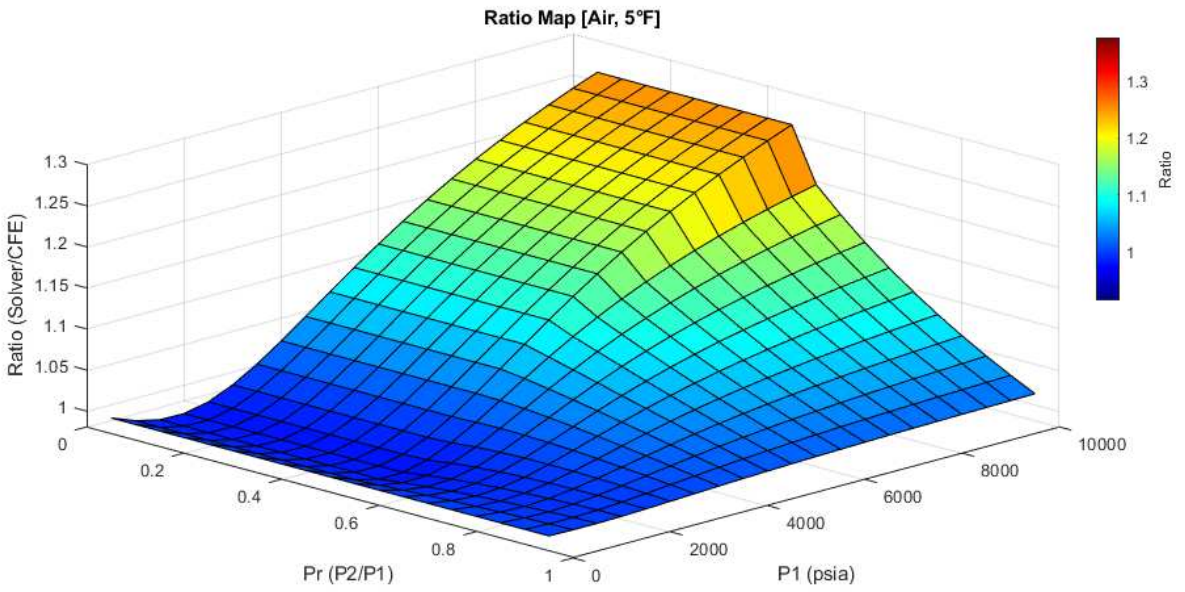

Figure 7 - Air Mass Flow Ratio v. Pr v. P1 5°F

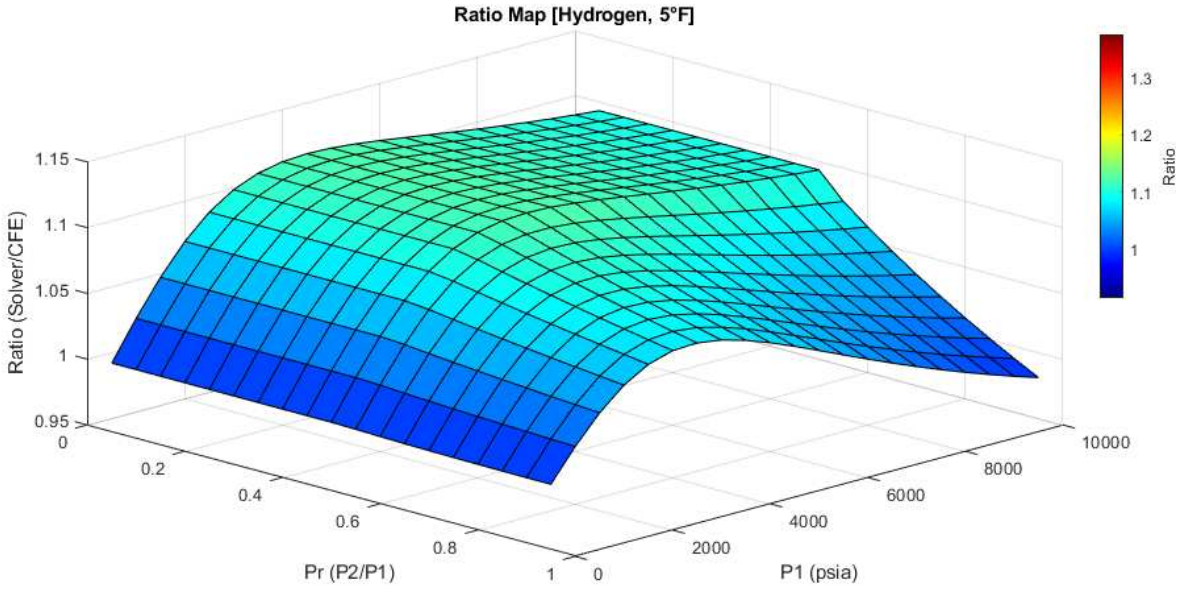

Figure 8 - Hydrogen Mass Flow Ratio v. Pr v. P1 5°F

Clearly, there is significant variation among the three shapes seen above, despite identical flow conditions for each point, other than varying gas type.

Real gas effects, as the name implies, are due to the difference between a real gas and an idealized gas. Therefore, we would expect to see less deviation from the ideal model in gasses that act more ideal. The primary factor responsible for the phenomenon dubbed real gas effects is intermolecular forces. In an idealized model of gasses, gas molecules are assumed to essentially consist of a single atom entity. When pushed to high pressures (such as 10,000 psi), the molecules of a real gas no longer follow this model exactly and should do so roughly proportional to the magnitude of their dissimilarity to the ideal one-atom gas. Based on this, we should see a trend between gas molecule size and dissimilarity to ideal behavior. Applied to the above maps, which were built to display a ratio of the real to ideal model, gas with molecules like methane (CH_4) that have more atoms with more mass and are less ideal, should see greater ratios (dissimilarity from an idealized model) when compared to the more ideal hydrogen (H_2). This is observed. As can be seen above, the Hydrogen map for the same flow conditions as Methane at 5°F sees a maximum ratio of 1.12 or a 12% deviation between the solver model and the ideal gas reliant isentropic equation, while Methane sees a maximum ratio of 1.43 or a 43% deviation between solver and CFE. This is a very significant deviation and appears to trend as expected. This can also be seen at higher temps, Figure 9 and Figure 10 below display the ratio maps for methane and hydrogen at 500°F. The methane map has a maximum deviation of around 9.5%, while the hydrogen map has deviation of around 1.5%, less than $\frac{1}{6}^{\text{th}}$ of the deviation of methane.

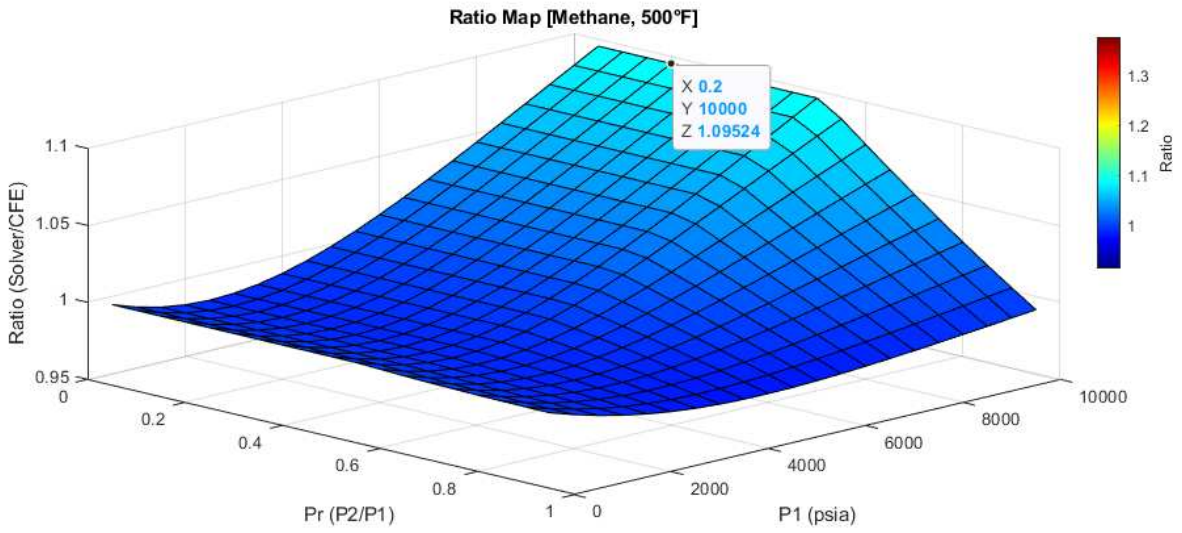

Figure 9 - Methane Mass Flow Ratio v. Pr v. P1 500°F

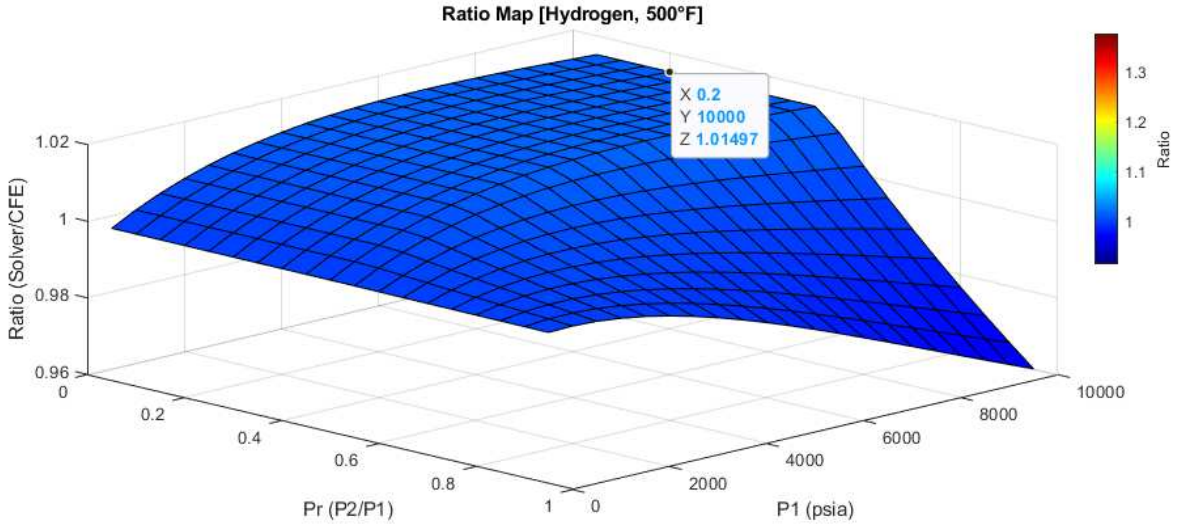

Figure 10 - Hydrogen Mass Flow Ratio v. Pr v. P1 500°F

4.2.2 Ratio Table vs. Temperature

Inlet temperature is another major factor in how ideal or non-ideal a gas behaves at some given flow condition. As explained above, the principal cause of the real gas behaviors that cause variance from an idealized model are intermolecular forces. Essentially, gas molecules,

especially larger ones such as methane, tend to develop an attractive or repulsive force in the direction of other molecules when compressed very tightly. This is not outside of the normal trend of material properties. When compressed sufficiently, real materials will develop significantly different properties moving from a gaseous phase to a liquid phase and eventually to a solid one. Increased temperature generally causes the opposite effect to an increase in pressure in this regard. As temperature increases, molecules, by definition, will have greater kinetic energy, which increases their repulsive force toward other molecules, overriding whatever intermolecular forces may be present due to molecular structure. Again, this fits the well-known trend of material properties. As a material is heated, given constant pressure, it will move away from a solid phase in which molecules are tightly locked to each other to a liquid phase where this is the less the case and eventually to a gaseous phase where its molecules are at their least bonded state. In the isentropic equation, some effort was made to capture this effect using the compressibility factor Z however, the following results indicate deviation that the compressibility factor is not capturing. Generally, this deviation appears to be in the direction of higher flow than predicted by the more ideal model.

The following are maps depicting the effects of temperature on gaseous air. The maps below display a ratio consisting of the solver mass flow rate divided by the isentropic compressible flow equation flow rate at a variety of flow conditions characterized by some

pressure ratio P_r of outlet pressure divided by inlet pressure and P1 or inlet pressure in psia. Each map is for some discrete temperature in Fahrenheit.

The first of these maps displays a significant amount of error at high pressures, with a 32.6% deviation between the solver model and the isentropic compressible flow equation model.

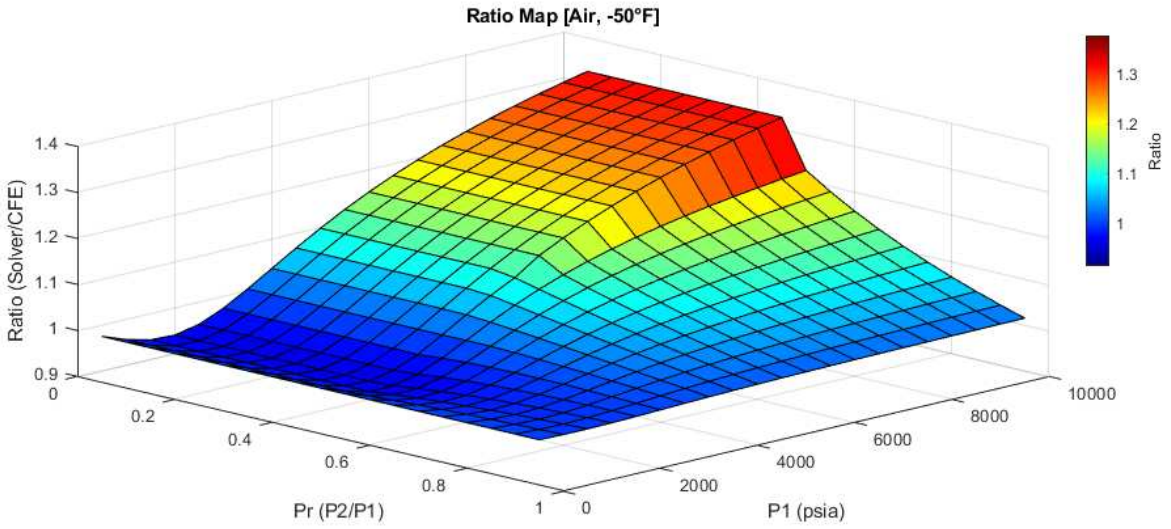

Figure 11 - Air Mass Flow Ratio v. Pr v. P1 5°F

It also displays significant variation in shape across the mapped surface. There is a significant dip in the 1000 psia pressure region of nearly -4% deviation (a ratio of 96.5) and a significant rise toward the higher pressure, topping out at 32.6% at 10,000 psia at the lower pressure ratios. It is also worth observing the relatively extreme slope of the map observed between the 0.45 and 0.5 pressure ratio planes. In addition to being a feature of the maps, this extreme slope is a topic that should be explored more in-depth as part of future work. An increased number of map points should be taken at this location.

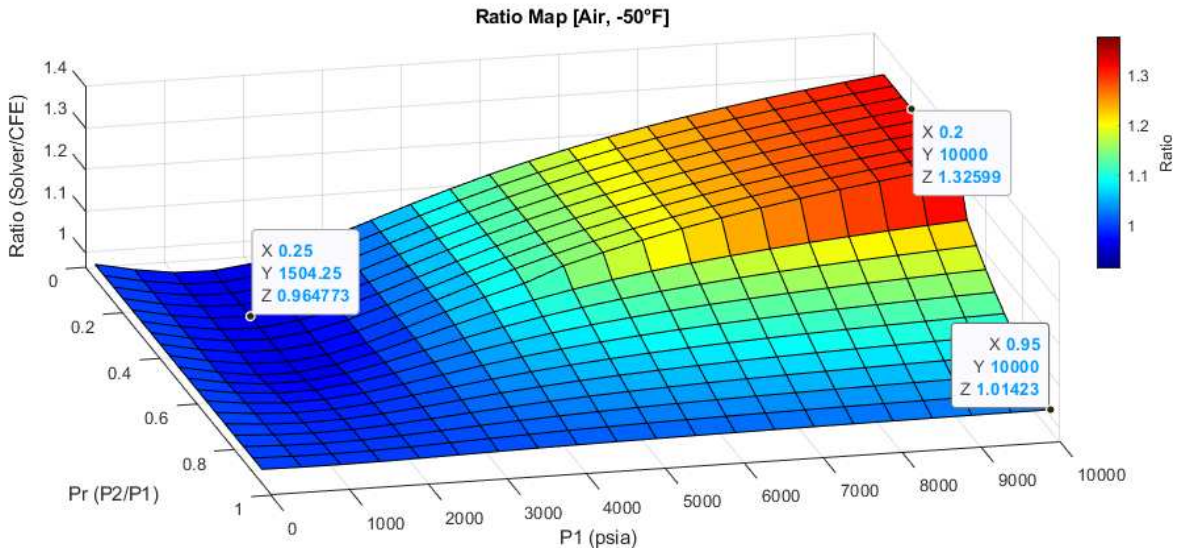

Figure 12 - Air Mass Flow Ratio v. Pr v. P1 5°F (altered view direction)

Taking all these facets of the -50°F Air ratio map into account, it is valuable to observe these features and their behavior as temperature increases. The map below in Figure 13 begins to demonstrate the overarching trend of the data. In this ratio map, the maximum ratio sits at around 1.26 or 26% variance between the solver and the isentropic compressible flow equation. The low point of the map sits at a solver/CFE ratio of around 0.98 or -2% variance. Comparing this to the 32.5% maximum and -3.5% minimum of the map displayed in Figure 12, a trend towards less variance begins to be apparent. To confirm the continuity of this trend of less variation with increasing temperature, ratio maps of higher temperatures should be examined.

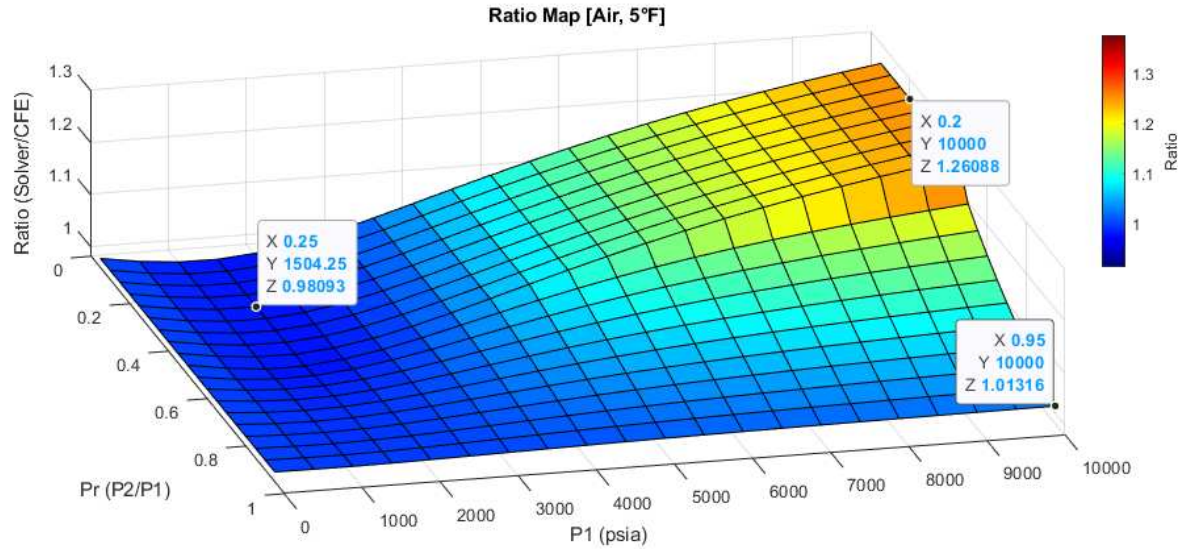

Figure 13 - Air Mass Flow Ratio v. Pr v. P1 5°F

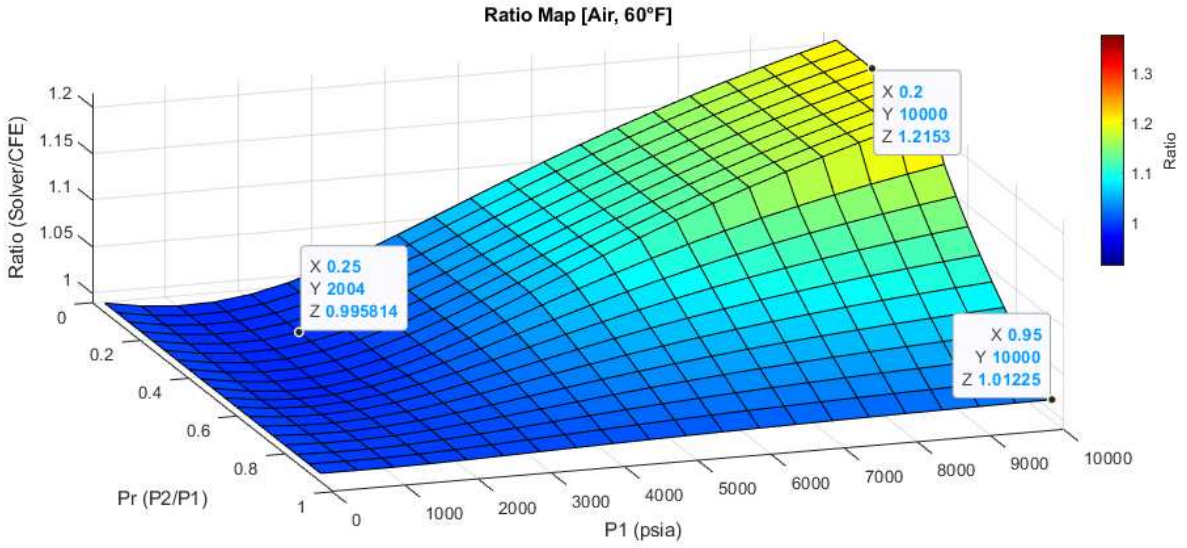

Figure 14 - Air Mass Flow Ratio v. Pr v. P1 60°F

Figure 13 and Figure 14 above both correlate with a general trend of less variation as temperature increases. The ratio map for air at 60°F shows a maximum variance of roughly 21% and minimum of roughly -1% (the marker in the figure above does not correlate to precisely this position as its aim was to show variance between maps at the same P_r and P1). This is a decrease of 11.5% on the maximum and an increase (and a corresponding decrease in magnitude) of 2.5%.

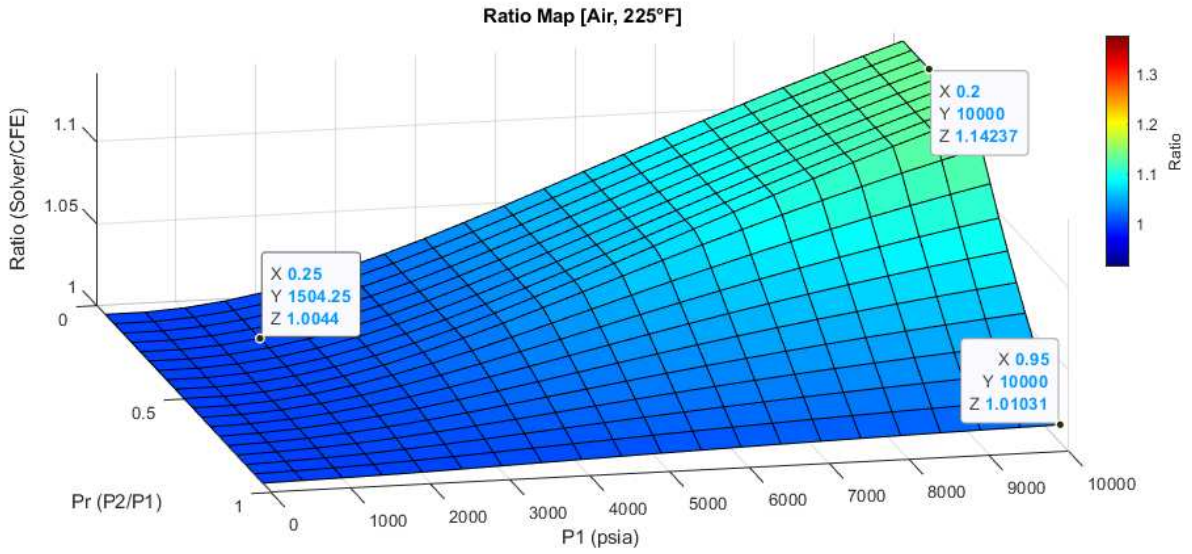

Figure 15 - Air Mass Flow Ratio v. Pr v. P1 225°F

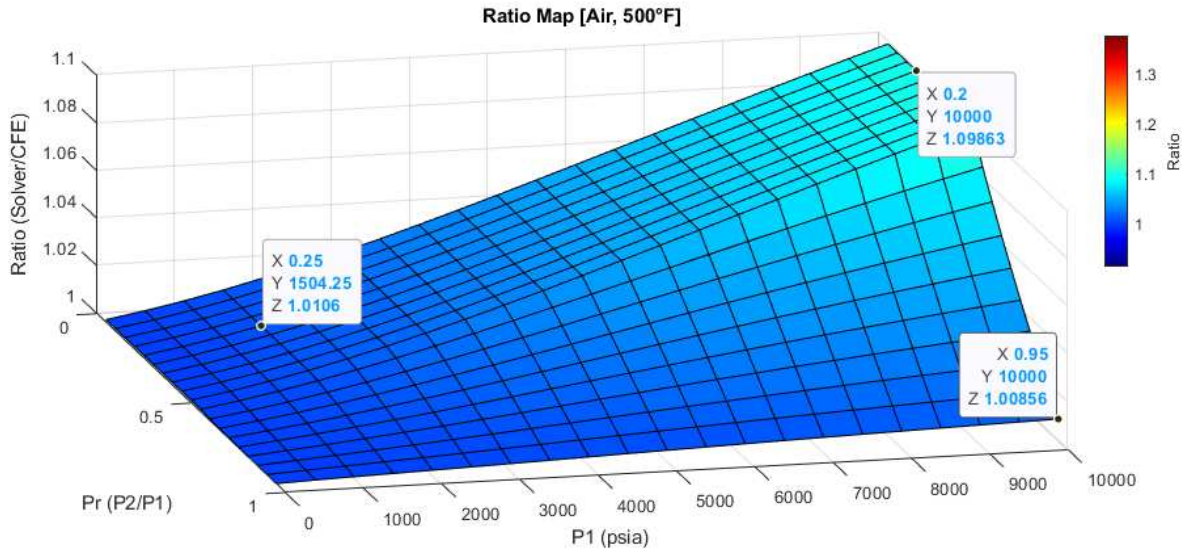

Figure 16 - Air Mass Flow Ratio v. Pr v. P1 500°F

This trend continues into the higher temperature ranges, eventually arriving at roughly a 10% maximum variance at 500°F with a minimum less than -0.05%. It is also worth noting here that the minimum pressure in the P1 direction is 5 psia as the solver and equation are both

incapable of running at 0 psia. 5 psia was selected due to its relatively insignificant shift from 0 psia in variance while still providing a baseline for when supercompressibility effects are negligible.

Given the results above, temperature's influence on the presence and magnitude of real gas effects is significant. Both the shape and relative magnitude of the deviation between the isentropic compressible flow equation and the solver changes by more than half of the maximum deviation over a span of 500°F and 10,000 psia and moves to a far more linear shape.

4.2.3 Temperature and Gas Type v. Ratio

The deviation between the more ideal isentropic flow equation and the solver shown above is useful within the context of a single gas. To extend this trend and explore its facets, it is worth comparing several different gas types and the trends of shape and magnitude change with changing temperature.

To begin the comparison of the gas types and their variation with increased temperature, it is assistive to understand the shapes of the ratio maps and deviation maps at a baseline temperature to more easily benchmark the effect temperature has on each gas's variation due to real gas effects from the baseline isentropic equation. To most effectively show this, a baseline temperature of -50°F is displayed below for Hydrogen, Air, and Methane.

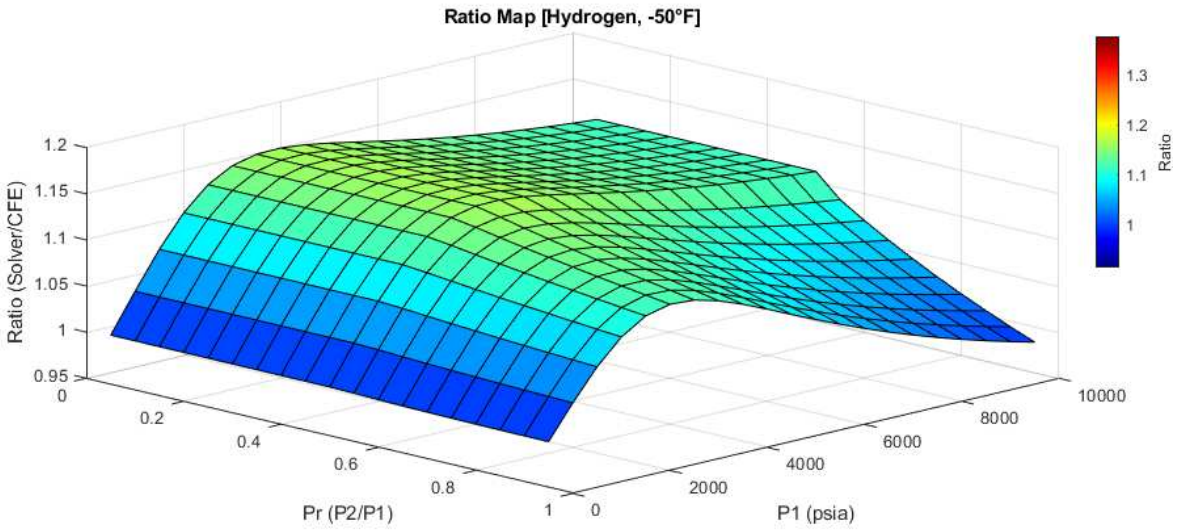

Figure 17 - Hydrogen Mass Flow Ratio v. Pr v. P1 -50°F

Observing the map of Hydrogen displayed in Figure 17, a deviation or ratio surface shape very different from that of methane and air is observed. There is a very clear rise in deviation in the positive direction that begins at 5 psia (effectively 0) and increases until around 3500 psia. This deviation then appears to taper off and then stabilize towards higher pressures.

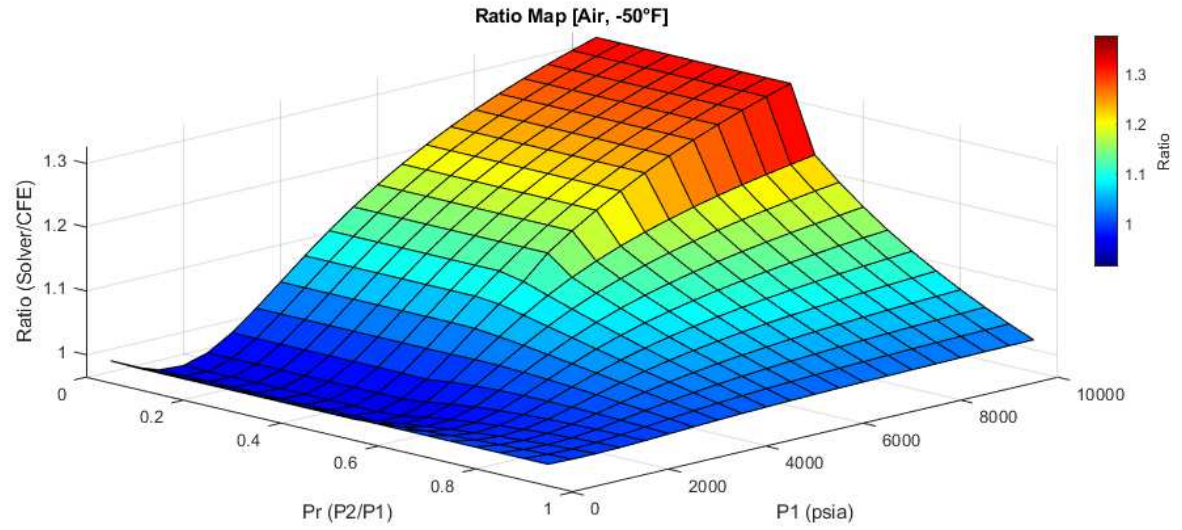

Figure 18 - Air Mass Flow Ratio v. Pr v. P1 -50°F

The ratio map for air at -50°F displayed above is displayed and described in some detail above in Figure 11. It is placed again here for continuity and easy comparison. In brief description, a relatively small negative deviation (or ratio under 1) is observed around 1000 psi. This then climbs much higher relatively in the sonic region (P_r < Alpha ≈ 0.475) landing at a maximum deviation over 30%. In the subsonic region, a slope towards 0 deviation or a ratio of 1 is observed as P_r increases. This slope roughly meets the sonic region deviation at the critical line (P_r = Alpha).

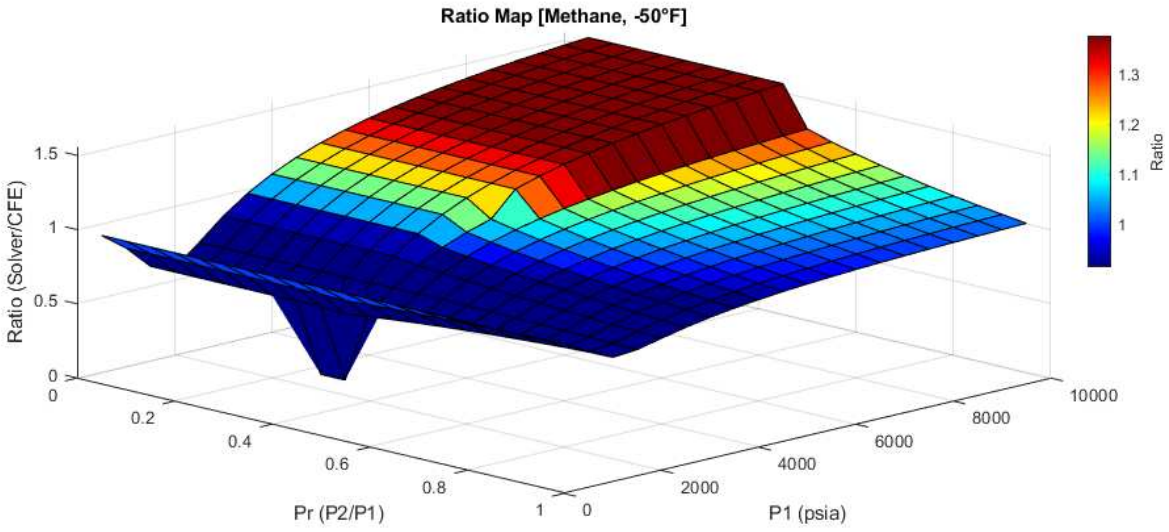

Figure 19 - Methane Mass Flow Ratio v. Pr v. P1 -50°F

Displayed above, Figure 19 depicts the deviation between the solver mass flow and isentropic compressible flow equation mass flow at -50°F. This ratio map has several interesting features. Largely around its seeming discontinuities. As noted elsewhere in this thesis, a finer mesh of points would be helpful in mapping exactly what trends look like at these points of seeming discontinuity. The most drastic discontinuity occurs around the 1500 psia P1 line and displays a ratio of around 0.2. By examining the error log generated by the solver when a trial is unable to converge, these trials appear to be faulty. This followed a general trend the solver had

of failing trials at low inlet temperatures and pressures like those seen above. This same trend occurs in similar carbon dioxide maps moving to higher temperatures. Based on trends seen during data collection, this is most likely due to fluid conditions in or very near the liquid phase of methane. The phase diagram for methane displayed below in Figure 20 indicates that the fluid is somewhere in the supercritical phase, not the compressible liquid phase. The red dot and arrow in the upper right of the figure display the location of these test points based solely on inlet conditions in the bar/°C scale. REFPROP indicated a similar fluid state based on P1 and T1, putting Methane in the supercritical phase. Despite this indication, the solver consistently has failed trials in this temperature, pressure, and P_r region for methane. One probable explanation for this failure is that the fluid undergoes fluctuations in temperature and pressure as it moves through the nozzle; these fluctuations likely trend in such a way that methane enters a liquid or near-liquid phase in these trials. This would likely have caused a failure to locate the fluid properties for methane in the REFPROP library, which in turn caused a solver convergence failure.

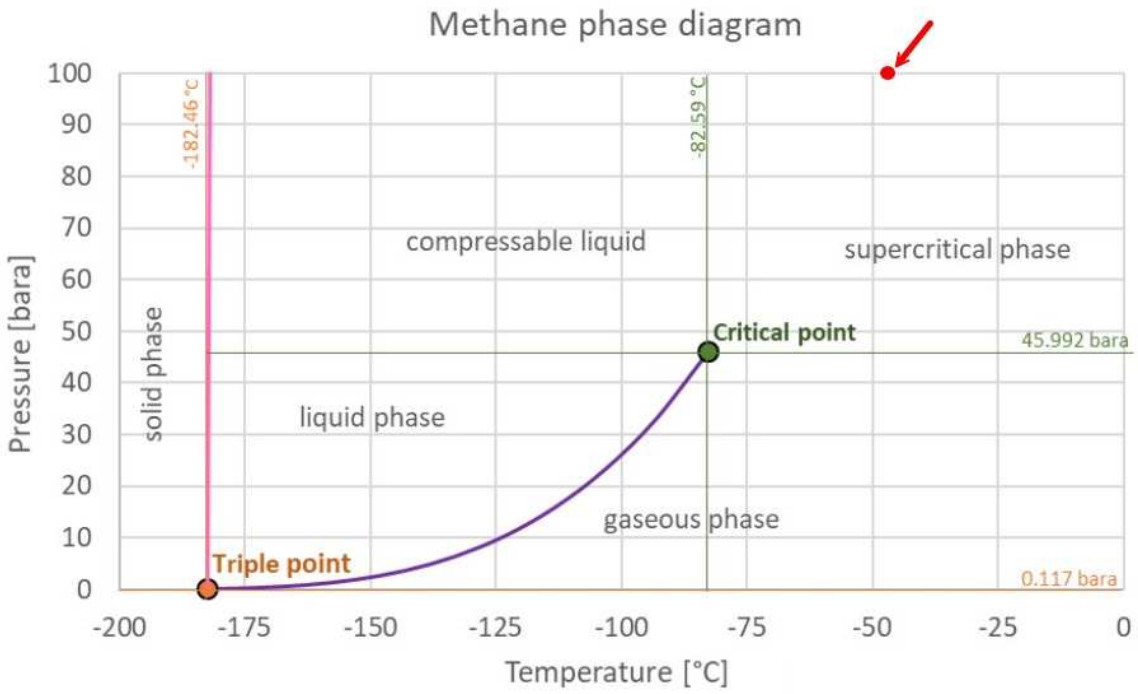

Figure 20 - Methane phase diagram Pressure (bara) v. Temp (°C)

4.2.4 Ratio Table vs. Inlet Pressure

Underlying all the shape and magnitude trends described above is an understanding that inlet pressure significantly affects the amount of real gas error experienced by a mathematical flow model based on the isentropic compressible flow equation at any given set of flow conditions. Observing all ratio maps in this thesis, there is almost no deviation between the solver model and the isentropic compressible flow model at the 5 psia mark on the data sets. Error across the full set of temperatures, pressure ratios, and inlet pressures does not exceed 0.5% deviation and is frequently much less. Given this, inlet pressure has the most significant role in creating real gas deviation from ideal behavior. This generally appears to align with the physics described above, as intermolecular forces that take effect due to molecular proximity are

understood to be the primary cause of real gas effects. Interestingly, these intermolecular forces do not appear to affect the mass flow deviation from the ideal gas model to the real gas model in a linear manner.

The ratio map for air at -50°F displayed below clearly demonstrates this non-linear deviation. Especially in the sonic region (lower P_r) Moving left to right from very low pressure to around 1500 psia there is a significant negative slope in ratio followed by a rise which eventually hits a point of inflection around 3000 psia. Moving further right, a strong positive correlation between inlet pressure and deviation between the solver and the CFE in the higher-pressure regimes takes place. It appears to begin to asymptote or linearize as it moves towards 10,000 psia. Given the extremely linear nature of the higher temperature maps, as shown in Figure 22, it is likely that this is the case; however, it is hard to tell without mapping the data to a higher pressure at the lower temperatures.

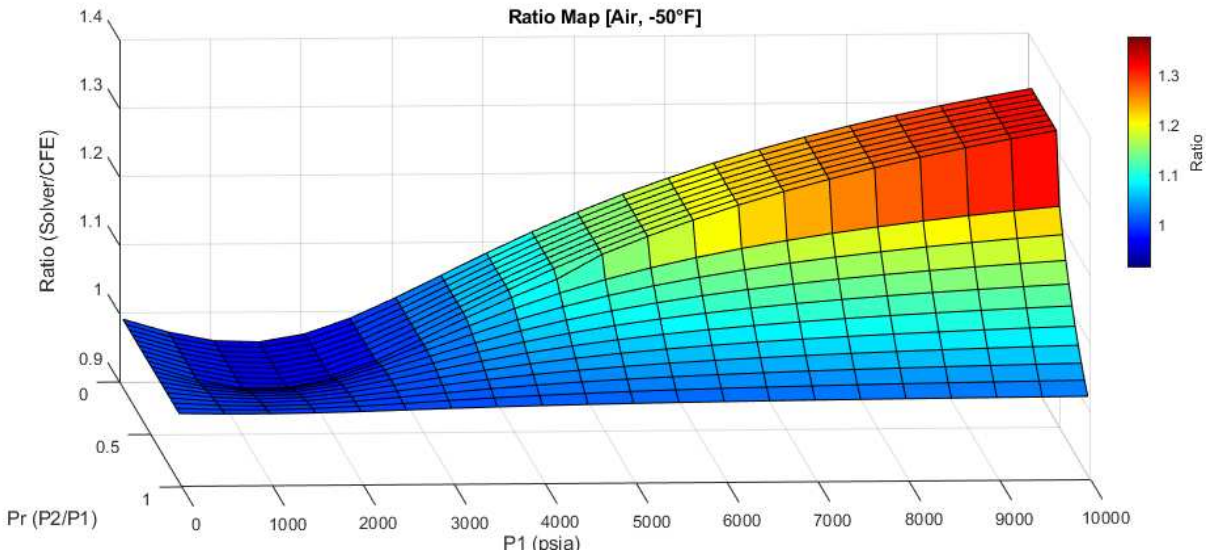

Figure 21 - Air Mass Flow Ratio v. Pr v. P1 -50°F (side profile)

As described above, the physical phenomenon held responsible for real gas effects regarding intermolecular forces should become more ideal with temperature. This does appear to be observed in Figure 22 below. The positive trend between inlet pressure and ratio appears to be far more linear at higher temperatures.

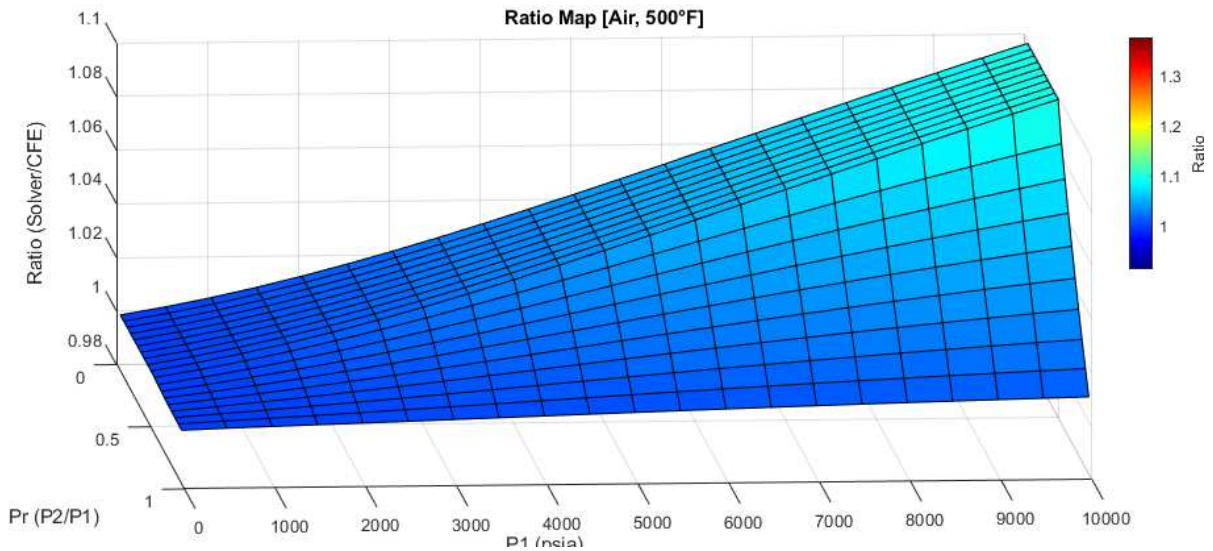

Figure 22 - Air Mass Flow Ratio v. Pr v. P1 500°F (side profile)

To further investigate this non-linear trend between P1 and deviation from the Isentropic Compressible Flow Equation low low-temperature ratio maps of methane (5°F) and hydrogen (-50°F) and high-temperature maps are displayed below in Figure 23, Figure 25, Figure 25, and Figure 26.

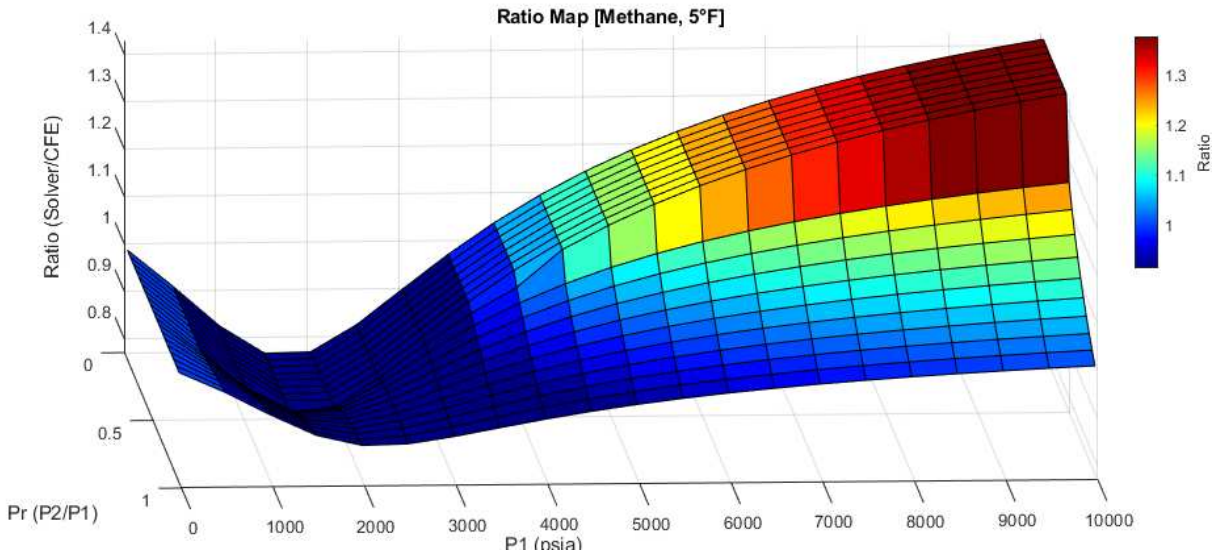

Figure 23 - Methane Mass Flow Ratio v. Pr v. P1 5°F (side profile)

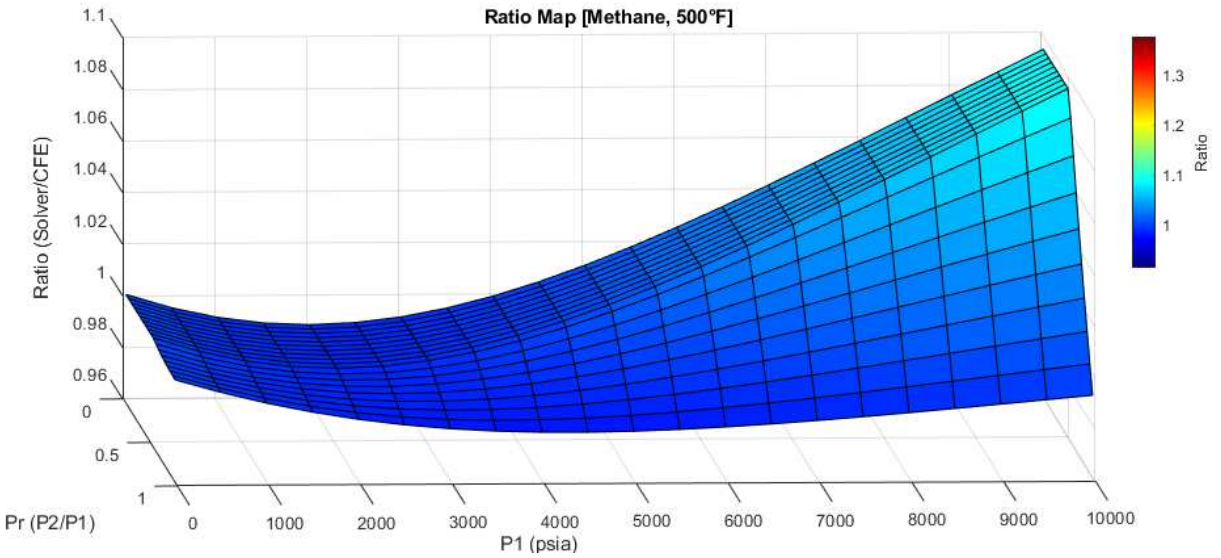

Figure 24 - Methane Mass Flow Ratio v. Pr v. P1 500°F (side profile)

Both high temperature and low temperature maps appear to exhibit a significant negative slope beginning at the 5 psia point on the map that extends until around 2000 psia moving from low to high P1. This low point appears to be in a very similar place along the P1 axis. Moving past the P1 = 2,000 psia plane, the low temperature map has a significantly more positive slope

that appears to become less positive approaching 10,000 psia plane. This positive trend also occurs for the high temperature map however it appears to be far more linear in nature.

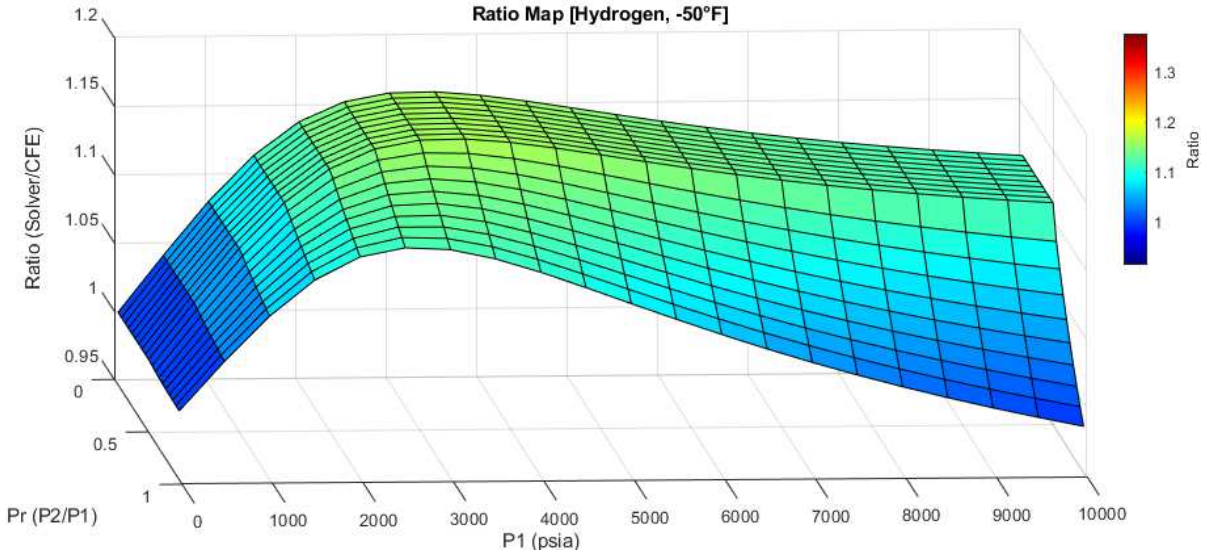

Figure 25 - Hydrogen Mass Flow Ratio v. Pr v. P1 -50°F (side profile)

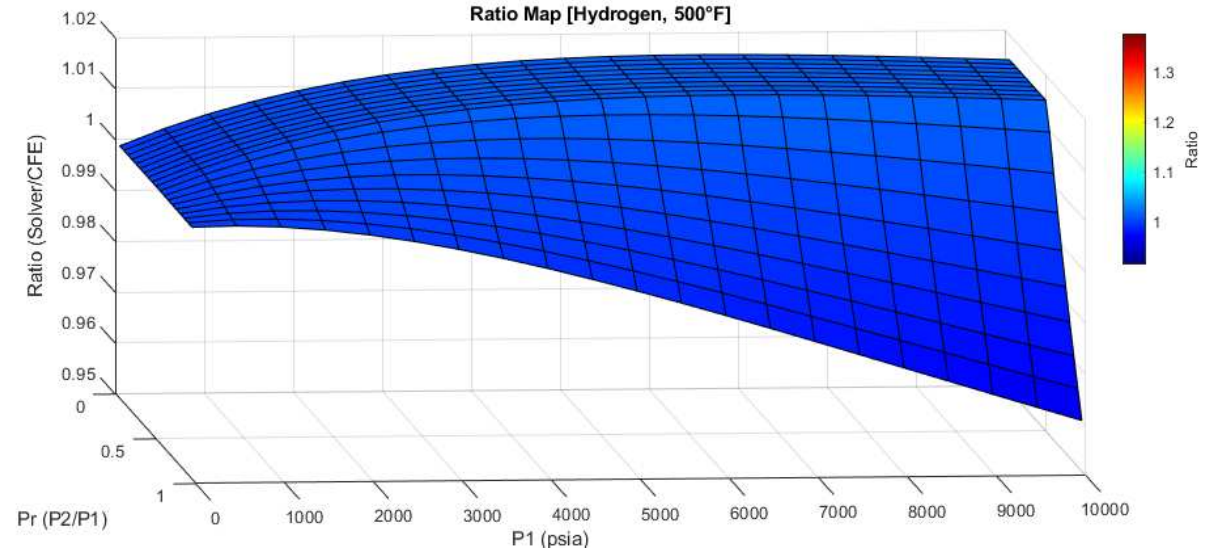

Figure 26 - Hydrogen Mass Flow Ratio v. Pr v. P1 500°F (side profile)

The hydrogen ratio maps displayed in Figure 25 and Figure 26 follow notably different P1 v. deviation than both the air and methane maps above. The lower overall magnitude of error is significant for hydrogen. The low-temperature (-50°F) methane and air maps have a maximum

ratio of ≈ 1.56 and ≈ 1.33, respectively, meaning the solver model for each has a variation of roughly 56% and 33% from the Isentropic Compressible Flow Equation baseline. The low-temperature (-50°F) hydrogen map has a maximum ratio of roughly 1.16 or 16% variation from the CFE baseline, indicating a maximum variation for hydrogen roughly half that of air and less than a third of methane's maximum variation. Given hydrogen's more ideal molecular structure, this aligns with the physics involved in real gas effects.

Another major difference between the hydrogen ratio maps seen in Figure 25 and Figure 26 and those of air and methane is the notable offset in the solver maximum deviation from the CFE. In the air and methane ratio maps, the maximum deviation occurs at the maximum P1 and shows signs of continued increase beyond this point, given no discontinuities at 10,000 psia (which is unlikely). In the hydrogen maps, this maximum occurs at around 3500 psia in the low-temperature (-50°F) map and 6500 psia in the high-temperature (500°F) map. This difference is significant and seems to indicate different levels of intermolecular attraction and repulsion among molecules of the same gas at different temperatures and even larger differences between dissimilar gasses.

4.2.5 Ratio Table vs. P_r

Per the ratio maps above, P1 has the most significant influence on the deviation between the solver model and the CFE model; however, it is followed closely by the effects of pressure ratio (the fraction P_r equal to $\frac{P_2}{P_1}$) on deviation from ideal behavior. P_r has a significant effect on the overall magnitude of the deviation given some P1 above relatively ideal pressures and on the shape of the deviation from the Isentropic Compressible Flow Equation Model. Additionally, certain facets of the shape of the ratio maps in regard to pressure ratio bring up questions as to

the accuracy of the model in the sonic-subsonic transition region and the validity of the assumption that the comparison of alpha and P_r is an effective way to predict the sonic transition at extreme pressures. Figure 27 below is a clear demonstration of this apparent discontinuity. Moving from 0.5 to 0.45 P_r there is a sudden jump in ratio or deviation of about 17%, significantly more than the deviation increase between points moving towards lower P_r in the sonic region.

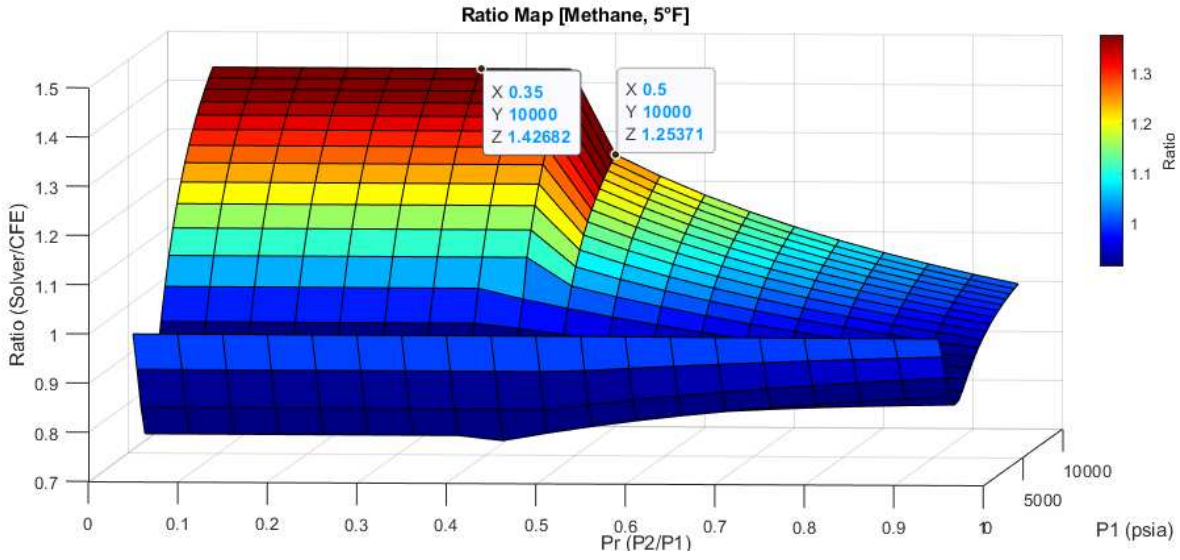

Figure 27 - Methane Mass Flow Ratio v. Pr v. P1 5°F (Pr Emphasized)

This can be seen more clearly, and the discontinuity can be confirmed to be a problem of exclusively the solver in the figures below. The Isentropic Compressible Flow Equation and EES solver are run on a set of 75 points run at the highest error case for Air, 10,000 psia and -50°F. These 75 points vary in P_r only to isolate potential discontinuity.

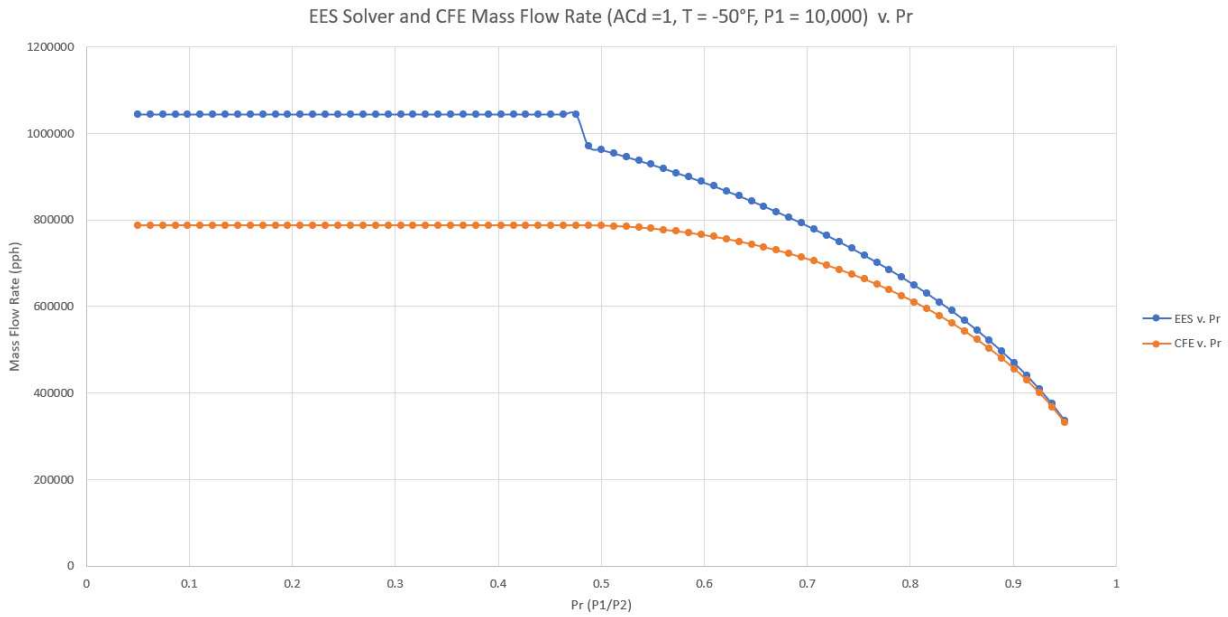

Figure 28 - EES and CFE v. Pressure Ratio (High Error Case)

As can be seen above, the solver has a very clear discontinuity at the point where P_r = Alpha, in this case at P_r = 0.47909. This is uncharacteristic of real phenomena and does not match the physical sonic transition.

CHAPTER 5: DISCUSSION

5.1 Validation

5.1.1 Isentropic Equation Comparison

As discussed previously, the Isentropic Compressible Flow Equation has been used as an industry standard for a long time and successfully predicts mass flow to within 1-2 percent of the actual tested value at pressures below 1000 psia. Extensive empirical testing has been done to confirm this. The empirical testing that has been done almost all centers around room temperature testing of air making the map below in Figure 29 applicable to almost all testing that has occurred.

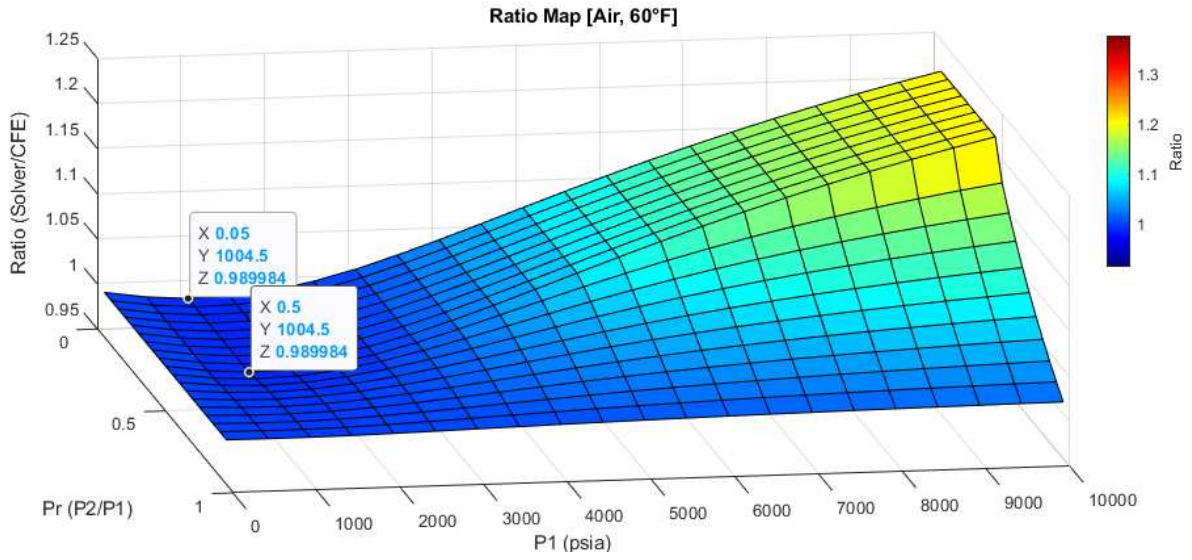

Figure 29 - Air Mass Flow Ratio v. Pr v. P1 60°F (Error in the sub 1000 psia region)

Extensive correlation testing was conducted during the creation of this thesis to ensure correlation between the solver and the isentropic compressible flow equation in this region. Through some relatively simple and robust rework, the solver method and CFE can both be manipulated to take mass flow as an input with ACd as an output. Much of the early validation

of the solver was conducted in this way. The map displayed below in Figure 30 demonstrates some of this validation. This map has different inputs from those displayed above, and the Error (%) axis refers to the deviation between the ACd generated by the CFE and the solver instead of mass flow as above. Despite this, the results have a very similar meaning. The test cases used to generate this map were made to mimic real test data that might be conducted on a research setup. Because of this, they provide a wider variety of flow conditions than the maps above and are more randomly varied.

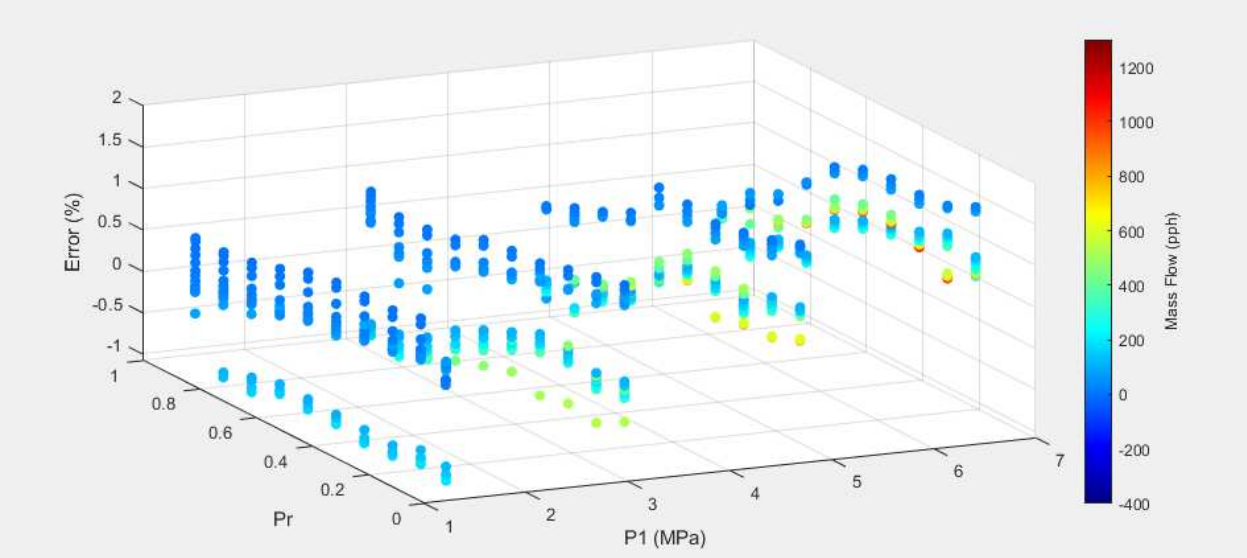

Figure 30 - Trial Data in Sub-1000 psia Range

The resulting error well within the 1-2 percent error range above can be combined with the understanding that the isentropic flow equation should be solid in this pressure regime to confidently state its validity at low pressures and its general functional operation. This does a great deal to prove the basic principles of the solver and lend it validity at higher pressures.

5.2 Significance

5.2.1 Improved Prediction Requirements

Several of the figures in the results section of this report indicate real gas error around 10% (and sometimes significantly greater in low temperature regions) in the 6000 psia range only on air.

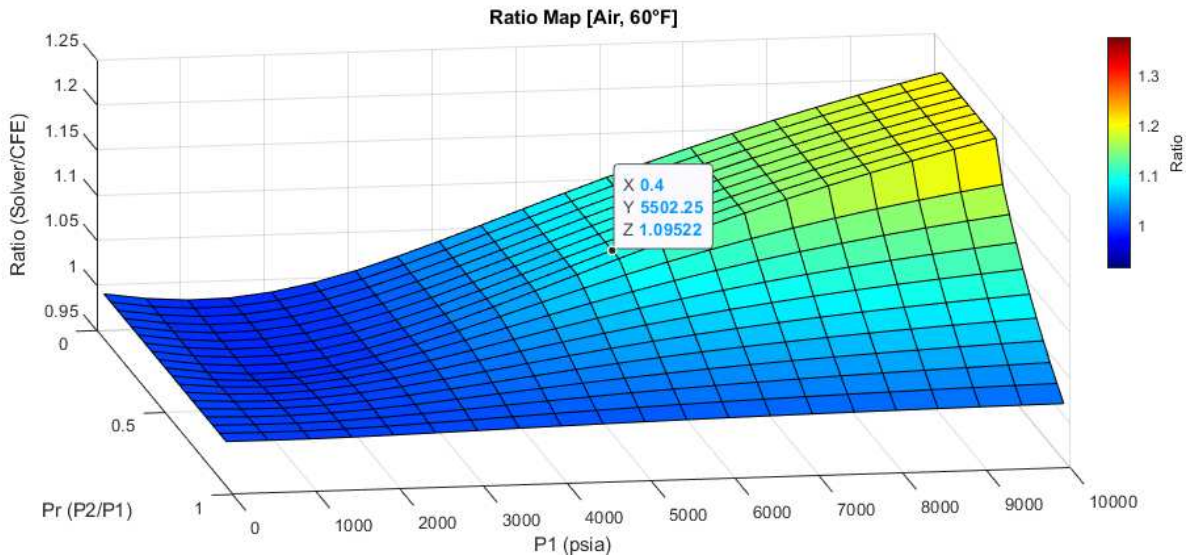

Figure 31 - Air Mass Flow Ratio v. Pr v. P1 60°F (Error at 6000 psia)

These error percentages appear to be slightly greater for methane in this same pressure range and significantly more for methane moving toward the very high pressures.

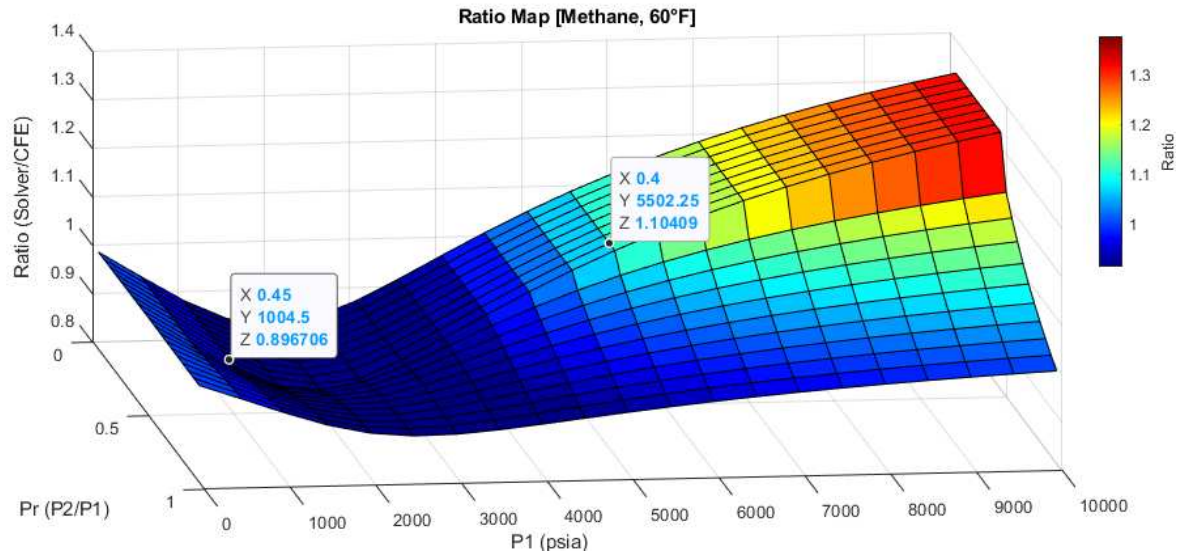

Figure 32 - Methane Mass Flow Ratio v. Pr v. P1 60°F (Error at 6000 psia)

For hydrogen, real gas effects have a smaller magnitude in the 6000 psia range however, they have a more significant effect at lower pressures.

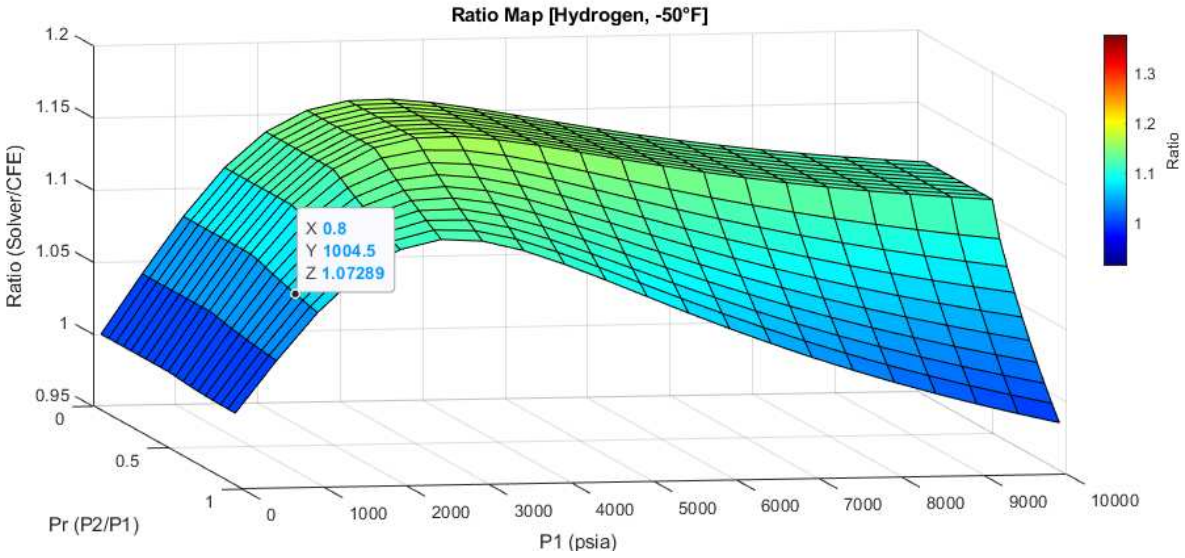

Figure 33 -Hydrogen Mass Flow Ratio v. P1 v. Pr -50°F (Error in the 1000 psia Range)

Figure 33 (though at a very cold temperature) demonstrates this clearly, showing the CFE to have more than 7% error in comparison to the solver at pressures around 1000 psia. Methane

displayed in Figure 32 has a similar early deviation, showing more than -10% deviation at 1000 psia at a relatively normal temperature.

5.2.2 Utilization of Calibration Fluids Given Gas to Gas Deviations

Based on all these findings, the consideration of real gas effects in precision mass flow prediction may have more effect than expected in today's control systems. Improved prediction appears to be critical once pressures increase to near 1000 psia for fluids other than air to achieve 1-2 percent error. Currently, the majority of valve calibration is done exclusively on air, and then these results are translated to other gasses. Based on the results of this thesis, this may not be an effective calibration strategy for pressures used with some frequency today.

Additionally, as applications such as super critical CO_2 cycles move further into popularity, real gas effect must be considered to reach accuracy anywhere near 1-2 percent. The 10% error that methane and air show at 6000 psia are of great consequence when trying to predict mass flow within 1-2 percent of reality.

This presents a challenge which should be solved if precision flow control with the use of a calibration fluid is to be attained. One potential solution for this involves the solver detailed in this thesis. Essentially, this thesis offers a theoretically more accurate solver model which is more capable of accounting for real gas effects. Generally, in the case of control valve production, industry calibration testing is used to determine a control valve's true effective area. Currently this is done via the isentropic flow equation or a similar equation susceptible to real-gas effect inaccuracies manipulated so that mass flow is a known variable and ACd is an output. The valve ACd is then back calculated. Then when the valve is in a use location, this ACd is used in conjunction with the mass flow output version of the isentropic flow equation to generate

a predicted mass flow value correlated closely to a real mass flow value (in current lower pressure cases). To make real-gas corrections to this strategy, the ratio maps above can essentially be generated for ACd instead of mass flow, computing real gas error at some baseline mass flow at a variety of flow conditions. This can then be used with flow data to generate a more accurate corrected valve ACd profile given the calibration fluid of choice. Then, when the valve is in an end use case, this strategy can again be used but with the original mass flow output real gas effect correction maps and the Isentropic Compressible Flow Equation to generate a predicted value more closely correlated to a real flow value. This second method using the solver should be more capable of accuracy given real gas effects as the solver correction factor should remove real gas inaccuracies from the flow data to ACd calculation and the ACd to flow data calculation.

5.2.3 Sonic-Subsonic Transition

An additional consideration that should be made, given the results above, is the validity of the assumption that flow through an orifice becomes sonic at P_r is equal to $\left(\frac{2}{k+1}\right)^{\frac{k}{k-1}}$ when pressure is greater than around 4000 psia. Based on a visual inspection of Figure 34, a clear inflection point that seems to be indicative of a discontinuity occurs between the 0.45 and 0.5 P_r plane. This lack of smoothness does not line up with the behavior of a real system and should be explored further.

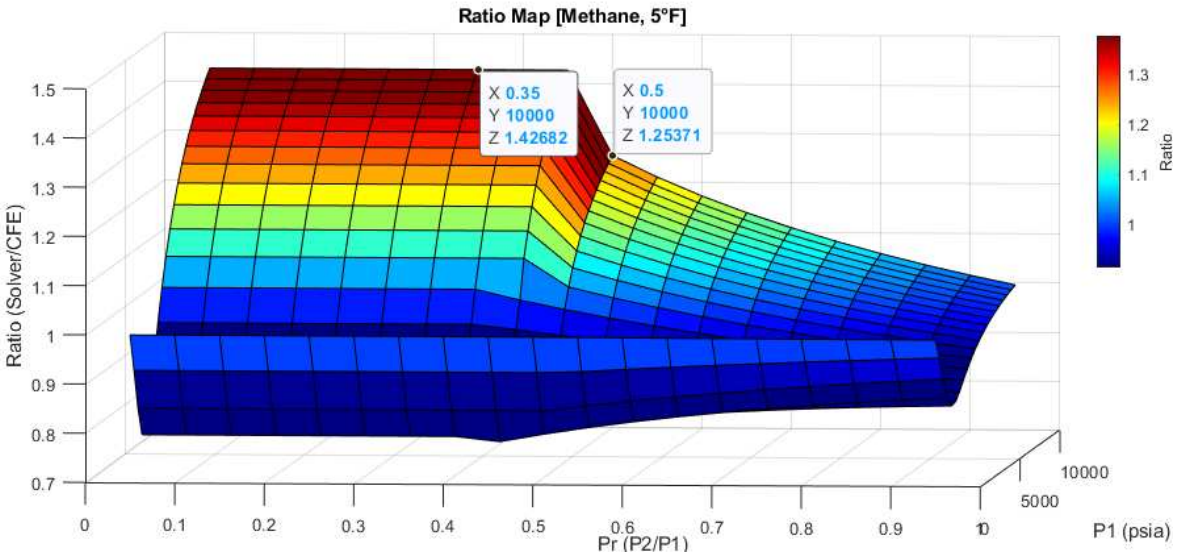

Figure 34 - Methane Mass Flow Ratio v. Pr v. P1 5°F (Pr Emphasized)

CHAPTER 6: CONCLUSION AND FUTURE WORK

6.1 Conclusion

At very high pressures, above 1000 psia, compressible fluids begin to deviate from ideal behavior due to phenomenon known as real gas effects. This thesis seeks to answer the question of how compressible mass flow through an orifice can be accurately characterized at extremely high pressures above 1000 psia. To do this, existing methods and their potential for inaccuracy at high pressure were examined. A more accurate method of prediction utilizing a solver and a large fluid property library was proposed and utilized in conjunction with the existing method to understand the deviation between the two methods. Significant deviation between methods was found to exist, especially among gasses with a less ideal molecular structure. A final method of prediction involving use of “ratio maps” combined with the existing Isentropic Compressible Flow Equation was proposed as an accurate method of mass flow prediction given knowledge of the gas flow conditions. A method of utilizing the “ratio mapping” above to link testing done with one fluid to that of another was also suggested offering a potential practical solution for continuing to use a calibration fluid to determine ACd and flow given conditions of a less known flow geometry.

6.2 Future work

Potential topics for future work on the topics presented in this thesis could take a variety of forms. The most logical next steps from the research presented here largely fall into a few categories: further validation of the solver, improvement of the solver tools' functionality and usability, and further documentation of the solver's function.

The first of these, the further validation of the solver, is the most pressing of the topics for further work. The contents of this thesis only show validation work up to roughly 1000 psi. This, combined with the solid fundamentals of the improvements in the solver, provide significant confidence that the results presented above are relevant, however, real physical test data at high pressures would help move the models presented above to a far more trustworthy state. If these results are to be used in the applications described above, this is a fundamental step of taking the results in this thesis to full applicability for industry and fields that rely on accurate flow prediction.

Ideally, an experiment to test the validity of real gas effects isolates sources of error and solely focuses on the true flow rate of a gas at known flow conditions through an orifice. The gas type, exact effective area of the test orifice, inlet pressure, outlet pressure, inlet temperature, and general system geometry should all be well known. Some variety of precision flow meter is also desirable to measure mass flow as this measurement is key. A test rig like the one documented in ISA 75.02.01, shown below as Figure *35* captures this idea [9]. The only potential difference to this system given the extreme pressure requirements is to move the flow meter downstream to an area where lower pressure is experienced. Flow meters are not often rated to the pressures that would be tested for this thesis, and they should be able to gather the exact same mass flow rate from downstream as upstream of the orifice.

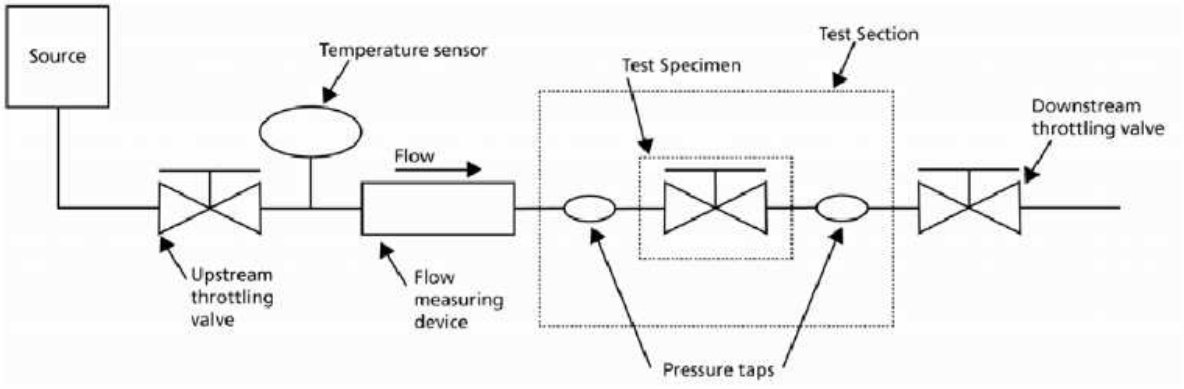

Figure 35 - ISA 75.02.01 Basic Flow Test System

One additional note here is that, ideally, a sonic nozzle would make up the test orifice as they generally have coefficients of discharge very near unity. Theoretically, they are at unity if friction effects can be avoided. This is never truly the case, but sonic nozzles can get extremely close to unity, especially when large in diameter. An example of this type of nozzle and its dimensions relative to the throat diameter is shown below in Figure *36*.

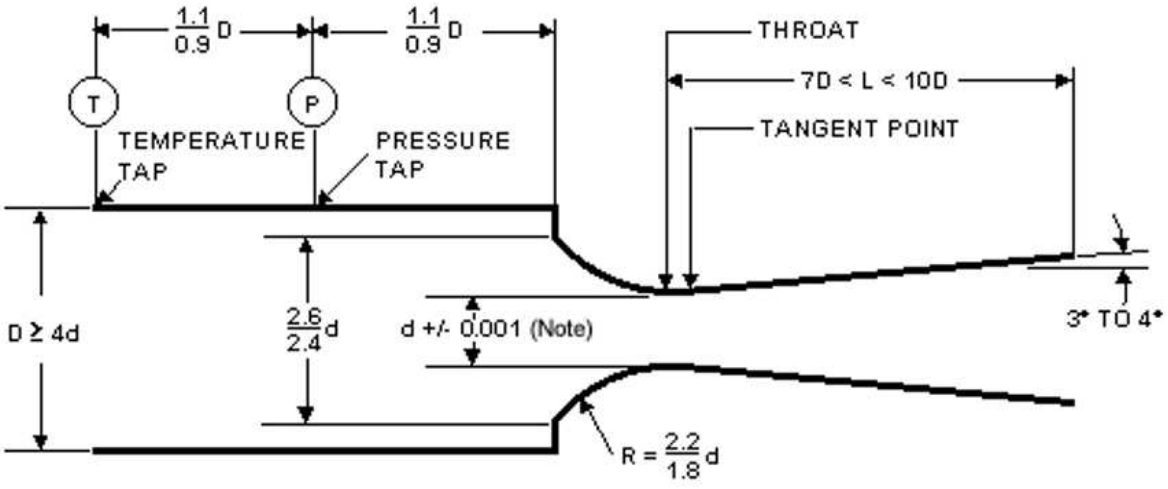

Figure 36 - ASME Toroidal Sonic Nozzle

Using this setup, one should be able to accurately calculate the real mass flow rate at high pressure and, using this and the precise ACd of the nozzle, determine the deviation in real gas

behavior from ideal gas behavior at high pressures. The procedure for this would essentially consist of comparing the real gas and ideal gas models (solver and CFE) for the predicted flow rate at high pressure. If the real gas solver model is more valid than the CFE it should more accurately predict the flow. An experimenter would also likely want to do tests at lower and more ideal gas pressures to determine the ACd of the nozzle and how friction effects may change with increased flow, as this may affect the results.

6.2.1 Solver improvements

Physical testing is extremely helpful in improving the validity of the results. However, the purpose of this thesis is fundamentally to understand how characterization and prediction can be conducted on compressible fluids. Because of this, the methods utilized to predict and characterize mass flow are also an important part of answering the underlying question of this thesis. Much of the approach taken and why it was taken is described above. The solver, as described above, does function, and the process for making the "ratio maps" used to help correct the isentropic flow equation with the goal of providing precise mass flow prediction is workable. Although this is true, there are several improvements to the functionality and utility of the solver that should be feasible to make, given the resources and time to do so. The highest value improvements and additions are recorded below.

- The ability to run the solver on user-defined gas mixtures could be added, specifically the addition of natural gas mixtures would add significant value for industrial applications requiring metering of such mixtures.
- EES has a feature called parametric tables, which are employed to do a series of calculations without requiring repeated input by the user. If used properly, this has the potential to greatly decrease the solver run time, allowing for much higher resolution

maps. There is some F-chart documentation noting methods of importing parametric tables; however, it has not been successfully incorporated into the solver as of the time of this thesis publication.

- The solver process currently involves several software tools, including Excel, EES, and MATLAB. The Excel portion could be incorporated into MATLAB code to streamline the overall process. EES is a key portion of the solver that would be difficult to recreate without significant time investment; however, with these improvements, the process could be streamlined to involve 2 software tools instead of 3.
- Plotting and an output folder containing the plots could be integrated.
- Add the equivalent of an if statement in the EES solver to make the sonic-subsonic choice solver operation based on a comparison of fluid velocity and the speed of sound for the fluid under the given conditions.
- Add consideration for viscosity and friction effects to the solver. For the approach above, this was assumed to be accounted for by ACd however research seems to indicate this may become a significant effect at high pressures and the solver does not adjust its results for this or contain any method for adjusting ACd or energy loss.

REFERENCES

1. "U.S. Energy Information Administration - EIA - Independent Statistics and Analysis." *Electricity in the U.S. - U.S. Energy Information Administration (EIA)*, www.eia.gov/energyexplained/electricity/electricity-in-the-us.php. Accessed 3 Mar. 2025.
2. Johnson, Robert C. "Calculations of real-gas effects in flow through critical-flow nozzles." *Journal of Basic Engineering*, vol. 86, no. 3, 1 Sept. 1964, pp. 519–525, https://doi.org/10.1115/1.3653160.
3. Lemmon, Eric W., et al. "Thermodynamic properties of air and mixtures of nitrogen, argon, and oxygen from 60 to 2000 K at pressures to 2000 MPA." *Journal of Physical and Chemical Reference Data*, vol. 29, no. 3, 1 May 2000, pp. 331–385, https://doi.org/10.1063/1.1285884.
4. MATSUO, Shigeru, et al. "Flow Characteristics of High-Pressure Hydrogen Gas in the Critical Nozzle" Saga University, Dept. of Mechanical Engineering, 2019.72, no. 0, 2019, https://doi.org/10.1299/jsmekyushu.2019.72.d15.
5. Mignot, Guillaume, et al. "Initial study of supercritical fluid blowdown." Fusion Science and Technology, vol. 47, no. 3, Apr. 2005, pp. 574–578, https://doi.org/10.13182/fst05-a747.
6. "Compressor Performance and Thermodynamics." Turbo Machinery Magazine, MJH Life Sciences, www.turbomachinerymag.com/view/compressor-performance-and-thermodynamic. Accessed 26 Mar. 2025.
7. Johansen, William R. "The Effect of Using Real Gas Absolute Viscosity And ..." IMEKO International Measurement Confederation, www.imeko.org/publications/tc9-2010/IMEKO-TC9-2010-071.pdf. Accessed 10 Apr. 2025.

8. Çengel, Yunus A., et al. Thermodynamics: An Engineering Approach. McGraw Hill, 2024.
9. ISA 75.02.01 - Control Valve Capacity Test Procedures | GlobalSpec, standards.globalspec.com/std/1178776/ISA%2075.02.01. Accessed 3 Mar. 2025.

6.3 MATLAB Live Script:

Below is the MATLAB live script used to calculate the "solver" portion of the results above and the ratios used to construct the maps in this thesis.

Mass Flow Calculator → ACd Input

Clear workspace and Command Window

```
clear
clc
```

Import From Excel File

Define path and location of input

```
f = waitbar(0, 'Building Input Matrices')
filename =
'J:\MastersProject\ACd_Input_Calc\ACd_Input\MATLAB_Input.xlsm'%'MATLAB_Input.xlsm
';
sheet = 'CarbonDioxide';
range = 'N2:I3269';
```

Read the matrix from the specified sheet and range

```
Test_Data_Full = readtable(filename, 'Sheet', sheet, 'Range', range);
Test_Data = readmatrix(filename, 'Sheet', sheet, 'Range', range);
```

Input Matrix Building

Define Input Variables:

1 2 3 4 5 6 7 8 9

| ACd | m_dot | P1 | P_Throat | T1 | k | SG | Z | Gas Type |

```
ACd_in2 = Test_Data(:,1) % in^2
m_dot_guess_pph = Test_Data(:,2) % pph   this is a guess for this calculator
P1_psia = Test_Data(:,3) % psia
P_Throat_psia = Test_Data(:,4) % psia
```

```
T1_R = Test_Data(:,5) % °Rankine
k = Test_Data(:,6) % Ratio
SG = Test_Data(:,7) % Ratio
Z = Test_Data(:,8) % Ratio
Gas_Type = Test_Data_Full(:,9) % Gas name formatted for EES
Inlet_Area_mm2 = 1000000 % 1664.575 % Upstream pipe area (1664.575 is utility) -
check
Rf = 0.75 % Temperature sensor recovery factor (0.75 is normal)
Pr = P_Throat_psia./P1_psia; % Ratio
Alpha = (2./(k+1)).^(k./(k-1)); % Ratio
```

Conversion Factors:

```
psia_to_MPa = 0.00689476 % psia to MPa
Rankine_to_Kelvin = 1/1.8 % Rankine to Kelvin
pph_to_kgph = 0.45359199999999533 % pph to kg per hour
in2_to_mm2 = (25.4^2) % in^2 to mm^2
```

Create EES Input Matrix:

Input Properties Column Names:

| 1 | 2 | 3 | 4 | 5 | 6 | 7 |

Gas Type P1 T1 ACd Inlet_Area Rf P_Throat

```
% Build 1 will be filled by gas type later
Input_Properties_Raw(:,2) = P1_psia * psia_to_MPa % MPa
Input_Properties_Raw(:,3) = T1_R * Rankine_to_Kelvin % Kelvin
Input_Properties_Raw(:,4) = ACd_in2 * in2_to_mm2 % mm^2
Input_Properties_Raw(:,5) = Inlet_Area_mm2 % mm^2
Input_Properties_Raw(:,6) = Rf % Unitless
Input_Properties_Raw(:,7) = P_Throat_psia * psia_to_MPa % MPa
% Convert to cell matrix and add Gas_Type
Input_Properties = num2cell(Input_Properties_Raw);
Input_Properties(:,1) = table2cell(Gas_Type);
[nrows,ncol]=size(Input_Properties);
```

Create New Output File:

```
% Destination Folder
folder = 'J:\MastersProject\ACd_Input_Calc\ACd_Input\Output_Log';


% Build File Name
baseFileName = 'Archive_Run_ACd_Input';
```

```
currentDate = datestr(datetime('now'), 'yyyymmdd_HHMMSS');
fileName = [baseFileName '_' currentDate '.xlsx'];


% File Path
filePath = fullfile(folder, fileName);


% Check for file of same name already in location and count name up:
counter = 1;
while isfile(filePath)
    fileName = sprintf('%s_%s_%d.xlsx', baseFileName, currentDate, counter);
    filePath = fullfile(folder, fileName);
    counter = counter + 1;
end


disp(['File created: ' fileName]);
```

Engineering Equation Solver Loop

EES Input/Output File Locations:

```
EESInput='C:\EES32\ACd_Input\From_MATLAB_ACd_Input.dat'; %input text file path
var
EESOutput='C:\EES32\ACd_Input\To_MATLAB_ACd_Input.dat';  %output text file path
var
```

Start Solver Timer

```
tic;
```

Make Blank Matrix for Solver and Error Log

```
Solver_Used = cell(nrows,1);
Error_Log = cell(nrows,1);
```

Set Error Out Time

```
Error_Out_Time = 10;
```

Run Correct EES Solver Based on Pressure Ratio

```
% Enter Loop
for row=1:nrows

    % Write Input File
    fid=fopen(EESInput,'w');  %open file for writing
    fprintf(fid,'%s %d %d %d %d %d %d\r\n',Input_Properties{row,:}); % write the
file properties
```

```
    fprintf(fid,'|Gas |  P1 (MPa)  |  T1 (K)     | ACd(mm^2) |Inlet Area(mm^2)|
Rf   |P2(MPa) subsonic |'); % Names
    fclose(fid); %close file
```

Subsonic

```
    %Run EES
    if Pr(row)>Alpha(row) %Pressure Ratio vs. Alpha
        % Run EES Subsonic from command line
        runtime = java.lang.Runtime.getRuntime();
        % J-drive and proper EES.exe
        % J-drive is 40% slower
        %process = runtime.exec('C:\Program Files (x86)\EES32\ees.exe /nosplash
J:\MastersProject\ACd_Input_Calc\ACd_Input\ACd_Input_Subsonic_V1.EES /solve');
        process = runtime.exec('C:\EES32\ees.exe /nosplash
C:\EES32\ACd_Input\ACd_Input_Subsonic_V1.EES /solve');
        completed = process.waitFor(Error_Out_Time,
java.util.concurrent.TimeUnit.SECONDS);


        if completed
            %disp('Process completed within 10 seconds.');
            Error_Log{row} = 'pass';
        else
            if process.isAlive()
                %disp('Done waiting for this...');
                process.destroyForcibly();
                disp('Process destroyed.');
                Error_Log{row} = 'fail';
            end
        end
        Solver_Used{row} = 'subsonic'; %Record which model was used
```

Sonic

```
    else
        % Run EES Sonic from command line
        runtime = java.lang.Runtime.getRuntime();
        process = runtime.exec('C:\EES32\ees.exe /nosplash
C:\EES32\ACd_Input\ACd_Input_Sonic_V1.EES /solve');
        completed = process.waitFor(Error_Out_Time,
java.util.concurrent.TimeUnit.SECONDS);


        if completed
            %disp('Process completed within 10 seconds.');
            Error_Log{row} = 'pass';
```

```
        else
            if process.isAlive()
                %disp('Done waiting for this...');
                process.destroyForcibly();
                disp('Process destroyed.');
                Error_Log{row} = 'fail';
            end
        end
        Solver_Used{row} = 'sonic'; %Record which model was used
    end
```

Rules:

Python must trust the folder it's in

EES solver must be in the same folder as the .dat file

```
    % Read File
    % Open the file written by EES and build prop columns
    output=dlmread(EESOutput);
```

| m_dot (kgph)| u1 (m/s) | Throat Temp (K)| SpdOfSnd (m/s)| C* |

```
    % Ouput Variable Definition
    m_dot_ACd_In(row,:)=output(1); %m_dot
    u1(row,:)=output(2); %u1 throat vel
    T_throat(row,:) = output(3); %T_throat Kelvin
    SpdSnd(row,:)=output(4); %Speed of Sound
    Cstar(row,:) = output(5); %C|star


    % Progress Tracking
    close(f)
    ProgressRatio = row./nrows;
    f = waitbar(ProgressRatio, 'Calculating...');

end
close(f)
```

Check Timer

```
elapsedTime = toc; % Stop the timer and get the elapsed time
timePer = elapsedTime/nrows;
```

```
fprintf('Elapsed time: %.2f seconds Time Per: %.2f seconds\n',
elapsedTime,timePer);
```

Isentropic Compressible Flow Equation Calculation

Begin For Loop:

```
for row=1:nrows %For loop of same size as the EES loop
```

Input Properties Column Names:

| 1 | 2 | 3 | 4 | 5 | 6 | 7 |

Gas Type P1 T1 ACd Inlet_Area Rf P_Throat

```
K1 = 3955.289; %Constant to make the units all work
P1_psia; %psia P1 matrix
P_Throat_psia; %psia P2 matrix
T1_R; %Rankine                % CAN REMOVE A LOT OF THESE
ACd_in2; %pph mass flow matrix   -  ACd now
Pr;  %pressure ratio matrix
k;   % k matrix
SG;  % SG matrix
Z;   % Z matrix
```

Define Variables for Use in Equation:

```
W_ACd = ACd_in2(row); %in^2
W_P1 = P1_psia(row); %psia
W_P2 = P_Throat_psia(row); %psia
W_K = k(row);
W_Sg = SG(row);
W_Z = Z(row);
W_T = T1_R(row)-459.67; %Fahrenheit


%VBA Paste
%Determination of R7 term (choked/ unchoked)
    if W_P2 / W_P1 >= (2 / (1 + W_K)) ^ (W_K / (W_K - 1))
        R7 = W_P2 / W_P1;
    else
        R7 = (2 / (1 + W_K)) ^ (W_K / (W_K - 1));
    end


%Flow formula
Comp_Flow_Eqn_Wf_pph(row,:) = W_ACd * (3955.289 * W_P1 * sqrt(((W_K * W_Sg) /
((W_K - 1) * (W_T + 459.67) * W_Z)) * ((R7 ^ (2 / W_K)) - (R7 ^ ((1 + W_K) /
W_K)))));
```

End For Loop:

```
end
```

Build Final Output Matrix

Close All Waitbars

```
close all
```

Calculate Error

```
Error = ((m_dot_ACd_In -
(Comp_Flow_Eqn_Wf_pph.*pph_to_kgph))./(Comp_Flow_Eqn_Wf_pph.*pph_to_kgph)).*100;
Error_Input = ((m_dot_ACd_In -
(m_dot_guess_pph.*pph_to_kgph))./(m_dot_guess_pph.*pph_to_kgph)).*100;
Ratio = m_dot_ACd_In./(Comp_Flow_Eqn_Wf_pph*pph_to_kgph)
```

Fill Final Output Matrix

```
% Copy in Inputs to Start of Output Matrix
Final = num2cell(zeros(nrows,21));
for col = 1:9
Final(:,col) = table2cell(Test_Data_Full(:,col));
end


Final_Array(:,10) = m_dot_ACd_In * 1/(pph_to_kgph);
Final_Array(:,11) = m_dot_guess_pph;
Final_Array(:,12) = Comp_Flow_Eqn_Wf_pph;                              % SHOULD ONLY
REPORT FOR SONIC
Final_Array(:,13) = Cstar;
Final_Array(:,14) = u1;
Final_Array(:,15) = SpdSnd;
Final_Array(:,16) = T_throat;
Final_Array(:,17) = Pr;
Final_Array(:,18) = Alpha;
Final_Array(:,19) = Error;
Final_Array(:,20) = Error_Input;
Final_Array(:,21) = Ratio
Final_Array = num2cell(Final_Array);
Final = [Final(:,1:9),Final_Array(:,10:21)];
```

```
headers = {'ACd (in^2)','m_dot Guess (pph)','P1 (psia)','P2 (psia)','T1
(°R)','k','SG','Z','EES Gas Type','EES m_dot (pph)','m_dot Guess (pph)','m_dot
WW_CFE (pph)','C*','u1','Speed of Sound','T Throat
(K)','Pr','Alpha','Error','Error_Input','Ratio'};
```

Input Properties Column Names:

| 1 | 2 | 3 | 4 | 5 | 6 | 7 | 8 | 9 |

ACd m_dot Guess P1 P_Throat T1 k SG Z Gas_Type

```
% Combine headers and matrix into a cell array
New2 = [headers; Final];
```

write to file

```
writecell(New2, filePath);
disp(['File created: ' fileName]);
```

Final Waitbar

```
f = waitbar(1, 'Calculation Completed');
```

Optional Plotting

```
%
% figure
% scatter3(P1e,Error,Pr,"red","filled")
% hold on
% % scatter3(Mass_Flow,ACd_Test_mm2,P1Final,"red","filled")
% % scatter3(Mass_Flow,ACd_Compare,P1Final,"green","filled")
%
% legend("EES","VBA","CFE") % EXTRA LEGEND ENTRIES ERROR
%
% title('Error v. Pr v. P1')
% xlabel('P1 (psi)')
% ylabel('Error')
% zlabel('Pr')
%
% hold off
%
% figure
% scatter3(Mass_Flow,m_dot_ACd_In,P1Final,"blue","filled")
% hold on
% scatter3(Mass_Flow,ACd_Test_mm2,P1Final,"red","filled")
% scatter3(Mass_Flow,ACd_Compare,P1Final,"green","filled")
%
% legend("EES","Input","CFE")
```

```
%
% title('MassFlow v. ACd v. P1')
% xlabel('Mass Flow')
% ylabel('Flow Area (mm^2)')
% zlabel('P1 (MPa)')
%
% hold off
%
%
%
% %plotXYZ(P1e, Pr, Mass_Flow, Error_Input,(min(Error_Input)),(max(Error_Input)),
'HP-Error', 'P1 (psi)', 'Pr','Mass Flow (kgph)','Error (%)')
```

```
function plotXYZ(x1, y1, z1, color1, col_lower, col_upper, plotTitle, xLabel,
yLabel, zLabel, clabel)


    % Create the scatter plot
    figure
    scatter3(x1, y1, z1, [], color1, "filled")
    colormap(jet); % Apply the 'jet' colormap
    colorbar; % Display colorbar
    title(plotTitle)
    xlabel(xLabel)
    ylabel(yLabel)
    zlabel(zLabel)


    % Add a label to the colorbar
    c = colorbar;
    c.Label.String = clabel;
    clim([col_lower, col_upper]);
end
```

```
%%%subprocess equiv testing
function runCommandWithTimeout(command, timeout)
t = timer('TimerFcn', @timeoutFcn, 'StartDelay', timeout);
start(t);
[status, cmdout] = system(command);
```

```
stop(t);
delete(t);


if status == 0
    disp('Command executed successfully:');
    disp(cmdout);
else
    disp('Command execution failed:');
    disp(cmdout);
end
end


function timeoutFcn(~, ~)
error('Command execution timed out.');
end
```

6.4 Sonic EES Script:

The script below is the sonic solver used to create the "solver" mass flow value in the ratio maps above.

```
$Import 'From_MATLAB_ACd_Input.dat' Gas_Type$ P1 Tm1 Flow_Area Inlet_Area Rf

"Relationship between static pressure and stagnation temperature for a given recovery factor:"
T1=(Tm1-Rf*To)/(1-Rf)

"Isentropic relation between stagnation and throat states:"
entropy(Gas_Type$,T=T_throat,P=P_throat) =entropy(Gas_Type$,T=To,P=Po)

"Energy balance between inlet stagnation and critical flow states:"
enthalpy(Gas_Type$,T=T_throat,P=P_throat)
+(soundspeed(Gas_Type$,T=T_throat,P=P_throat))^2/2=enthalpy(Gas_Type$,T=To,P=Po)

"Isentropic relation between stagnation and throat states:"
entropy(Gas_Type$,T=To,P=Po) =entropy(Gas_Type$,T=T1,P=P1)

"Energy balance between stagnation and inlet states:"
enthalpy(Gas_Type$,T=T1,P=P1) +u1^2/2=enthalpy(Gas_Type$,T=To,P=Po)

"Conservation of mass between inlet and the critical flow area:"
u1=density(Gas_Type$,T=T_throat,P=P_throat)*(Flow_Area/Inlet_Area)*soundspeed(Gas_Type$,T=T_th
roat,P=P_throat)/density(Gas_Type$,T=T1,P=P1)

"Mass Flow through the throat:"
```

```
m_dot=density(Gas_Type$,T=T_throat,P=P_throat)*soundspeed(Gas_Type$,T=T_throat,P=P_throat)*36
00[s/hr]/(1000[mm/m])^2*Flow_Area

"Stagnation Compressibility Factor For Output:"
Zo=compressibilityfactor(Gas_Type$, T=To ,P=Po)

"Speed of Sound to Print"
SpdSnd = soundspeed(Gas_Type$,T=T_throat,P=P_throat)



"Calculate Critical Flow Factor:"
C|star=density(Gas_Type$,T=T_throat,P=P_throat)*soundspeed(Gas_Type$,T=T_throat,P=P_throat)*((R
*To)^.5)/(Po*1E6 [Pa/MPa])
MW=molarmass(Gas_Type$)                    "Molecular Mass for Gas Selected"
Ru=8314.4598 [J/K-kmol]                    "Universal Gas Constant"
R=Ru/MW                                    "Specific Gas Constant"

$Export 'To_MATLAB_ACd_Input.dat' m_dot u1 T_throat SpdSnd C|star
```

LIST OF ACRONYMS

8. CFE – Isentropic Compressible Flow Equation
9. ISA – International Society of Automation
10. NASA – National Aeronautics and Space Agency
11. NIST – National Institute of Science and Technology
12. REFPROP – REFerence fluid PROPerties
13. EES – Engineering Equation Solver
14. MATLAB – MATrix LABoratory